The chemical behavior of fluids released during deep subduction based on fluid inclusions

MARIA LUCE FREZZOTTI[1] AND SIMONA FERRANDO[2]

[1] Department of Earth and Environmental Sciences, University of Milano Bicocca, Piazza della Scienza 4, 20126 Milano, Italy. e-mail: maria.frezzotti@unimib.it

[2] Department of Earth Sciences, University of Torino, Via Valperga Caluso 35, Torino 10125, Italy. email: simona.ferrando@unito.it

Revision 2

ABSTRACT

This review combines fluid inclusion data from (H*P*-)UH*P* rocks with experimental research and thermodynamic models to investigate the chemical and physical properties of fluids released during deep subduction, their solvent and element transport capacity, and the subsequent implications for the element recycling in the mantle wedge. An impressive number of fluid inclusion studies indicate three main populations of fluid inclusions in H*P* and UH*P* metamorphic rocks: i) aqueous and/or non-polar gaseous fluid inclusions (FI), ii) multiphase solid inclusions (MSI), and iii) melt inclusions (MI). Chemical data from preserved fluid inclusions in rocks match with and implement "model" fluids by experiments and thermodynamics, revealing a continuity behind the extreme variations of physico-chemical properties of subduction-zone fluids. From fore-arc to sub-arc depths, fluids released by progressive devolatilization reactions from slab lithologies change from relatively diluted chloride-bearing aqueous solutions (± N_2), mainly influenced by halide ligands, to (alkali) aluminosilicate-rich aqueous fluids, in which polymerization probably governs the solubility and transport of major (e.g. Si and Al) and trace elements (including C). Fluid inclusion studies point to a reconsideration of the petrological models explaining deep volatile liberation, and their flux into the mantle wedge.

INTRODUCTION

The chemical behavior of fluids in deep subduction zones and its implications for element cycling and flux melting in the mantle wedge, which causes the formation of arc magmas, has been a subject of growing interest in the last twenty years (e.g., Manning 2004; Bebout 2007, 2013). Experimental and theoretical research represents a major tool for understanding the chemical and physical properties of slab-derived fluids, and for modeling the metamorphic evolution of deep subducting rocks (e.g., Ulmer 2001; Poli and Schmidt 2002; Manning 2004; Sanchez Valle 2013; and references cited).

Closely related to theoretical and experimental research are studies of fluid inclusions in metamorphic rocks. High pressure (H*P*) and ultra-high pressure (UH*P)* eclogite-facies rocks of crustal origin represent an excellent natural laboratory for the study of subduction-zone fluids, since they underwent pressure and temperature conditions comparable to those hypothesized to occur in deep subducting slabs (Carswell and Compagnoni 2003). A large number of fluid inclusion studies in eclogites and related rocks have reported a remarkable variety of fluid types: aqueous fluids with variable halide content ± non-polar gases (e.g., N_2, CO_2, CH_4), aluminosilicate-rich aqueous fluids, intermediate between silicate melt and water, and hydrous silicate melts (c.f., Scambelluri and Philippot 2001; Touret and Frezzotti 2003; Ferrando et al. 2005; and references cited). Many among these inclusions have lost their original composition, but some still preserve the chemistry of fluid trapped during prograde and peak UH*P* metamorphic conditions, despite subsequent exhumation from extreme depths. In this paper, we highlight how fluids in inclusions can constrain and explain deep subduction processes. After providing a review of current research on fluid inclusions in (H*P*-) UH*P* metamorphic rocks, we express our view on the chemical and physical characteristics of subduction-zone fluids preserved as inclusions, including solvent and element transport capacity, and implications to

cycling of volatiles. Further recent discussion on fluid inclusions in UH*P* metamorphic rocks can be found in Scambelluri and Philippot (2001), Touret and Frezzotti (2003), Ferrando et al. (2005), Zheng et al. (2011), Klemd (2013), and Hermann et al. (2013).

FLUID INCLUSIONS IN H*P*-UH*P* METAMORPHIC ROCKS

Fluid inclusions are tiny volumes of mobile volatile-rich phases trapped in minerals during, or after their growth (Roedder 1984). For this reason, they represent the only possible way to acquire firsthand information on naturally occurring fluids. A digest of current main research on fluid inclusions in UH*P* eclogite-facies metamorphic suites is provided in Table 1. It summarizes different pieces of information, including inclusions' main textural (stage of trapping, inclusion type, and host minerals) and chemical (daughter minerals, water *vs.* gas) characteristics, along with the nature of host metamorphic rocks (metamorphic belt, peak *P*-*T* conditions, matrix lithologies). A synthetic report of the interpretations proposed by the single authors is included. Most examples are on primary fluid inclusions (i.e., fluid inclusions trapped during growth of the host mineral; Roedder 1984) in peak metamorphic minerals of crustal rocks, that, as a consequence, preserve the composition of the hydrous fluid phases released by the slab at more than 90 km depth, during deep subduction (i.e., *P*-*T* stability field of coesite).

Three distinct populations of fluid inclusions are observed in H*P* and UH*P* metamorphic rocks (Table 1): i) chloride-bearing aqueous and/or non-polar gases fluid inclusions (FI), ii) multiphase solid inclusions (MSI), and iii) melt inclusions (MI). We will deliberately be avoiding the term '*polyphase* inclusion' often reported in literature as an alternative to MSI (see, Table 1), since this definition applies to any inclusion containing

more than two phases (e.g., a fluid inclusion containing liquid H_2O, liquid CO_2, and gaseous CO_2 is defined as a polyphase inclusion) and may cause confusion.

Chloride-bearing aqueous, and/or non-polar gaseous fluid inclusions (FI)

Chloride-bearing aqueous fluid inclusions (FI) are observed in H*P* and UH*P* eclogite (Svensen et al. 1999, 2001; Xiao et al. 2000, 2002; Fu et al. 2001; Shen et al. 2003; Ferrando et al. 2005a; Mukherjee and Sachan 2009), eclogitic veins and segregations (Philippot and Selverstone 1991; Selverstone et al. 1992), quartzite and whiteschist (Philippot et al. 1995; Ferrando et al. 2009), Mn-rich garnet nodules (Frezzotti et al. 2011), and garnet pyroxenite (Fu et al. 2003a; Table 1). FI are small (< 40-50 μm in diameter) and show irregular, rounded, or negative crystal shapes. Although some biphase (liquid + vapor) liquid-rich FI are reported (e.g., Ferrando et al. 2005b), most of them are three-phase (solid + liquid + vapor) inclusions with about 40-90% of the total volume consisting of liquid + vapor (Figs. 1b - d).

As evident from Table 1, one (e.g., halite) to three chlorides are generally observed (Fig. 1c), often associated with carbonates (e.g., calcite, Mg-calcite, dolomite, hydrous carbonates), and/or minor sulfates (mainly gypsum), sulfides (mainly pyrite), and oxides (rutile, ilmenite). More rarely, phosphate (apatite, monazite) and silicate (amphibole, mica, epidote, quartz, feldspars, kyanite, omphacite, ellenbergerite, glaucophane; Fig. 1d) daughter minerals have been described. Interestingly, FI in garnet nodules from Lago di Cignana (Italian western Alps) contain several carbon phases (carbonate, diamond, graphite, carbonaceous material) and an aqueous fluid bearing HCO_3^-, CO_3^{2-}, and SO_4^{2-}, ions, and silica monomers in solution, but no chlorides (Fig. 1b).

Non-polar gaseous fluid inclusions are observed in eclogite (Fu et al. 2001; Xu et al. 2006; Mukherjee and Sachan 2009) and garnet pyroxenite (Fu et al. 2003a; Table 1). These tiny

inclusions (< 10 μm in diameter) are single-phase pure (N_2, or CH_4) or binary (N_2-CH_4, rarely CO_2-N_2) mixtures, gray to dark in color due to their low refractive index. Commonly, they are associated with chloride-bearing aqueous fluid inclusions (Fu et al. 2001). Mixed N_2-CO_2-CH_4-H_2O ± solids inclusions (Fig. 1a) are reported from H*P* eclogite (Fu et al. 2003b; Xiao et al. 2001, 2002), garnet pyroxenite (Fu et al. 2003a), quartzite (Frezzotti et al. 2007), and whiteschist (Philippot et al. 1995; Table 1). The gas bubble volume is variable from < 20 to > 80 % of the inclusion. These inclusions occur isolated (Frezzotti et al. 2007), or in association with chloride-bearing aqueous fluid inclusions (Fu et al. 2003a). Halite is the most common mineral phase in these inclusions, although gypsum, anhydrite, and pyrite have been locally reported (Table 1).

Multiphase solid inclusions (MSI)

Multiphase solid inclusions (MSI; Table 1) are peculiar primary inclusions present in peak mineral assemblages of UH*P* rocks, recognized in eclogite (Ferrando et al. 2005 a, 2005b) and eclogitic veins (Zhang et al. 2008), felsic gneiss (Stöckhert et al. 2001, 2009; Dobrzhinetskaya et al. 2003a, 2003b, 2012), quartzite (Frezzotti et al. 2007; Ferrando et al. 2005b), Grt-Cpx-Qtz rocks (Hwang et al. 2003), whiteschist (Philippot et al. 1995; Ferrando et al. 2009), marble (Hwang et al. 2005, 2006), garnet pyroxenite (van Roermund et al. 2002; Carswell and van Roermund 2005;Vrijmoed et al. 2008; Malaspina et al. 2010), garnet peridotite (Malaspina et al. 2006, 2009), and Ol-Opx rocks (Scambelluri et al. 2001).

MSI show variable sizes (from 5 to ca. 100 μm in diameter), and polygonal or negative crystal shapes (Figs. 2 and 3). At room temperature, they consist of aggregates of 4 to10 different solid phases of relatively large sizes, with subordinate fluid, or empty cavities (< 40% of the total volume of the inclusions; Figs. 2a and 2b). Most of the solid phases are hydrous (alkali) aluminosilicate minerals (white micas, talc, chlorite, phlogopite, biotite, amphiboles, epidote *s.l.*,

ellenbergerite, staurolite), though anhydrous silicates (quartz, feldspars, zircon, kyanite, pyroxenes, titanite, olivine, kalsilite) are also observed (Table 1). Carbonates (mainly calcite, Mg-calcite, dolomite, magnesite) constitute common, subordinate phases. Minor sulfates (mainly gypsum and anhydrite), or sulfides (mainly pyrite), phosphates (mainly apatite and monazite), and oxides (mainly rutile and spinel *s.l.*) can also be present (Table 1). Reduced carbon phases (diamond, graphite, disordered carbonaceous material) are observed in some localities (Stöckhert et al. 2001; van Roermund et al. 2002; Dobrzhinetskaya et al. 2003a, 2003b, 2012; Carswell and van Roermund 2005; Vrijmoed et al. 2008; Stöckhert et al. 2009; Malaspina et al. 2010; Table 1)Chlorides are rarely present (Philippot et al. 1995; Hwang et al. 2005, 2006; Ferrando et al. 2009; Table 1).

In MSI, the relatively large solid phases, in particular lamellar minerals, show intimate intergrowths and preferred orientations, often resulting from periodic crystallization (Figs. 2a, 2c, 2d, and 3). Textural relationships of daughter minerals are different from those observed in crystallized MI in plutonic and in H*T* metamorphic rocks (i.e., "stone cavities" in granites, and "nanogranites" in migmatites; Sorby 1858; Frezzotti 1992; Cesare et al. 2009). In MSI, crystallization of daughter phases appears to have started in the center of the inclusion cavity and proceeded to the walls, exponentially increasing mineral surface. Crystallization seems to have occurred from a homogeneous relatively low-viscosity melt or fluid, by processes such as diffusion mass transport and growth (e.g., periodic precipitation; Liesgang phenomena). Locally, granoblastic textures, and rare developments of triple joints among equant and prismatic minerals are also observed (Figs. 2b).

In contrast to the previous class of FI, it is difficult to optically detect liquid water in MSI (Figs. 2 and 3) due to: i) the high amount of solid phases in the inclusions, ii) the high density of the trapped fluids, and iii) the possibility that water passively diffused from inclusions during the retrograde evolution of the host rocks (see following paragraphs). Microthermometric analyses

collected in MSI with a relatively high amount of fluid indicate a solute-rich aqueous solution (e.g., Zhang et al. 2005). Non-polar gas species, such as N_2 and/or CO_2 have not been detected by Raman microspectroscopy (Table 1).

Melt inclusions (MI)

Melt inclusions (MI) can occur in quartz-feldspatic rocks and garnet-bearing gneiss (Hwang et al. 2001, 2006; Mposkos et al. 2009), metapelite (Lang and Gilotti 2007), Grt-Cpx rocks (Hwang et al. 2004, 2005), marble (Korsakov and Hermann 2006), eclogite (Shen et al. 2003; Gao et al. 2012), garnet peridotite (Naemura et al. 2009; Table 1). They form by decompression melting of eclogite-facies matrix rocks during early retrogression, or by local *in-situ* dehydration-melting of hydrous mineral phase inclusions within prograde and peak minerals (see also, Klemd 2013).

In general, MI in UH*P* metamorphic rocks are recrystallized, similarly to what observed in plutonic or in H*T* metamorphic rocks, although, most unexpectedly, minor volumes of glass have been reported in a few cases (e.g., Hwang et al. 2004; Hwang et al. 2006; Table 1). During slow cooling in the Earth's crust, crystallization of silicate phases inside MI typically initiates on the cavity wall, and the nucleation rate is greater than the growth rate, resulting in the formation of a number of randomly-oriented fine-grained, anhedral to subhedral crystals of similar size (Fig. 4; Frezzotti 2001). In UH*P* rocks, MI are generally small (ca. 10-50 μm in diameter), with polygonal or negative crystal shapes, generally filled by tiny aggregates of feldspars, micas, and quartz, or, more rarely, of carbonates, and carbon phases ± silicates (Table 1). In particular, these inclusions show magmatic textural relationships, such as an order of crystallization, or graphic intergrowths (e.g., Korsakov and Hermann 2006; Mposkos et al. 2009), similar to (crystallized) MI in plutonic and H*T* metamorphic rocks. Fine-grained mineral assemblages are also observed

to partly or totally replace former phengite lamellae because of their *in-situ* dehydration melting (e.g., Gao et al. 2012; Liu et al. 2013). Finally, irregular pockets filled by relatively coarse-grained reactants and products of dehydration melting reactions involving phengite are also reported in UH*P* rocks (Lang and Gilotti 2007).

POST-ENTRAPMENT MODIFICATIONS OF H*P*-UH*P* FLUID INCLUSIONS AND MULTIPHASE SOLID INCLUSIONS

UH*P* FI and MSI are usually trapped during the growth of the host mineral (primary or early inclusions; Roedder 1984; Touret 2001). They occur isolated or as clusters and, if abundant, they are regularly distributed (Fig. 5a) marking the growth zones of the host mineral (Fig. 5b). The fidelity of the FI and MSI fluid record is based on two fundamental assumptions. The first one is that their chemistry must be representative of the composition of the fluid phases present in the system at trapping conditions (Roedder, 1984). Because of the constant proportions of crystallized minerals (Fig. 2 and 3), most FI and MSI appear to have trapped an homogeneous UH*P* fluid phase. Exceptions, are represented by those inclusions which contain incidentally-trapped minerals. These last ones are recognizable for their nonsystematic occurrence and, typically, for having larger dimensions than daughter minerals (Fig. 5c). Similarly, in MI, presence of magmatic mineral assemblages, replacing a hydrous phase during its *in-situ* dehydration melting, and/or of reactants and products of a dehydration melting reaction are a strong evidence for incipient anatexis of UH*P* rocks, but are not representative for the composition of the melt generated during this event.

The second assumption requires that, after trapping an homogeneous fluid phase, inclusions behaved as closed systems, i.e. they evolved independently from the host minerals

(Roedder 1984; Touret 2001). Post-trapping modifications can affect some inclusions and spare some others nearby (Fig. 6). This depends on the nature of the host mineral, and on the size, shape and location (i.e., dislocations in the host) of the inclusions in the host mineral (Viti and Frezzotti 2000; 2001; Touret 2001; Frezzotti and Ferrando 2007; Stöckhert et al. 2009).

As illustrated in Fig. 7, crystallization of daughter minerals (stage 2 of Fig. 7) during decompression does not necessarily imply changes in the chemical composition of the former fluid. In some cases, also the retrograde chemical interaction between the inclusion and the host mineral does not affect the chemical composition of the former fluid. For example, the negative crystal shape shown by most inclusions (Figs. 2, 3 and 6) develops just after the entrapment by dissolution and precipitation of the host mineral on the inclusion walls (stage 2 of Fig. 7). This is an equilibrium process that is not considered to modify the former fluid composition (e.g., Roedder 1984; van den Kerkhof and Hein 2001; Frezzotti 2001). Similarly, retrograde metamorphic reactions inside MSI (e.g., pseudomorphosis, hydration reactions; Figs. 6 or 8a, respectively; stage 4 of Fig. 7) do not change the chemistry of the former fluid (Frezzotti et al. 2012a).

In contrast, *non-equilibrium* growth of the host mineral on the inclusion walls (typically with slightly different composition) can modify the chemical composition of both the trapped fluid and the host mineral that crystallizes on the inclusions walls (e.g., Heinrich and Gottschalk 1995; Frezzotti 2001). This evolution is commonly observed in MSI (and MI) which were subject to high-*T* conditions during the retrograde evolution (stage 3 of Fig. 7). Retrograde metamorphic reactions between the host mineral and the inclusions on cooling (e.g., hydration reactions) and diffusion of elements from the inclusions, can modify significantly the composition (Fig. 8a and d), and changes in the oxygen fugacity of the inclusion fluid may also occur. Chemically re-equilibrated MSI (Fig. 6 and 8c-f) are easy to recognize, since they show irregular contours typically forming re-entrant angles, and can contain newly formed minerals

(i.e., step-daughter minerals; e.g., Svensen et al. 1999; Ferrando et al. 2005b; Stöckhert et al. 2001, 2009).

Due to the strong decompression during retrograde evolution, decrepitation (i.e., burst by explosion) represents another very common post-trapping process in both FI and MSI. This process modifies the former density of the fluid. Decrepitation occurs when the host mineral is no more able to accommodate the pressure difference in and out of the inclusion ($\Delta P = P_{in} - P_{out} >> 0$; Fig.7) (e.g., Touret 2001; Franz et al. 2001; Stöckhert et al. 2009). FI in elogite-facies rocks can re-equilibrate their density at different *P-T* conditions several times during decompression (Fig. 7; e.g., Touret 2001; Touret and Frezzotti 2003; Frezzotti and Ferrando 2007; Stöckhert et al. 2009).

In MSI, early UH*P*-H*P* retrograde decrepitation (stage 3 of Fig. 7) can be identified by irregular contours and short and large fractures (offshoots) departing from the inclusion corners (Figs. 6, 8a, 8e, 9a, 9c, 9d), similarly to fluid inclusions in mantle xenoliths (Fig. 9b). On the contrary, decrepitation at lower *P* (stage 5 of Fig. 7), liberating a fluid phase when all minerals have already crystallized (stage 4 of Fig. 7), generally forms: i) star-shaped contours (Figs. 6, 9d-e), and/or ii) haloes of very small FI distributed around the inclusion (Fig. 9c), and/or iii) short trails of tiny secondary FI lining from the decrepitated inclusions (Fig. 8c-d). These petrographic features are similar to those observed in volatile-rich MI in plutonic rocks, undergoing volatile oversaturation and magma degassing during slow cooling after trapping as inclusions (Fig. 9f).

ELUSIVE AND FUGITIVE WATER

A careful petrographic study is necessary to select those UH*P* inclusions potentially representative for the chemical composition of the metamorphic fluids. The determination of the

248 water content of the former fluids is more problematic. In most MSI, water represents an elusive
249 and fugitive component, although empty spaces between hydrous daughter minerals (Fig. 8a)
250 testify for the (former) presence of an aqueous fluid component. A valuable way to study water
251 speciation inside MSI is by spectroscopic techniques. One possible analytical approach is
252 described in Frezzotti et al. (2010). In Fig. 10, synchrotron FT-IR maps show the speciation of
253 water in MSI both as H_2O molecules (Fig. 10b) (i.e., liquid phase; absorption bands in the 3000–
254 3500 cm^{-1} region, Fig. 10e), and as OH^- groups (Fig. 10c) (i.e., in daughter mineral phases;
255 absorption bands in the 3500–3800 cm^{-1} region, Fig. 10e). Comparing Figs. 10a and 9b, the
256 systematic absorption increase in the 3000–3500 cm^{-1} region in correspondence of MSI reveals
257 that, in contrast with the optical observation, they may contain some liquid water. Quantitative
258 analyses, however, are not possible.

259 An additional concern is that the low-water content of MSI could result from passive H_2O
260 diffusion during the retrograde *P-T* evolution. MSI can exchange H_2O with the host minerals if
261 the internal P_{H2O} in the inclusion is higher than the external P_{H2O} (or X_{H2O}) of the fluids
262 circulating in the rocks (Sterner and Bodnar, 1991), a very common case during retrograde
263 decompression at relatively high temperatures (Fig. 7). If decrepitation does not occur, the
264 inclusion fluid P_{H2O} can passively re-equilibrate with the external fluid conditions. Identifying
265 MSI dehydration, if present at all, would also require spectroscopic investigations. The example
266 in Fig. 10d shows a synchrotron FT-IR map of hydrogen distribution in pyrope (Frezzotti et al.
267 2012a and b). Exponential enrichment of bonded hydrogen in garnet approaching MSI reveals
268 the change from molecular water in MSI to OH^- bonds to the anhydrous host. Hydrogen
269 gradients, recorded by symmetrically different colored haloes, represent actual water content
270 variations in garnet, with the exception of the MSI area where the extremely high water
271 concentration in garnet in part results from a MSI contribution (yellow to pink haloes in Fig.
272 10d). Fluid inclusion "dehydration" processes were previously proposed to interpret the origin of
273 some pure CO_2 FI in peridotite xenoliths, formed at depths of about 60 - 80 km and rapidly

brought to the surface by erupting magmas (Hidas et al. 2010; Frezzotti et al. 2012a). In these rocks, thermodynamic modeling (MFSHC system) of observed reactions between FI and surrounding minerals suggested a potential H_2O content in mantle C-O-H fluids variable from 10 to 50 mole %, lost from FI after trapping in minerals (Frezzotti et al. 2012a).

These results suggest that the amount of fugitive water from inclusions formed at high *P-T* conditions may not be trivial, and that MSI could have contained tens of mole % H_2O, most of which - if not all - potentially lost during early retrograde decompression in matrix rocks. Extending this process to FI, we hypothesize that some of the highly saline compositions described in the previous paragraphs (e.g., Fu et al. 2001; Ferrando et al. 2005a; Zhang et al. 2005; Xiao et al. 2006; Mukherjee and Sachan 2009), could also result from selective H_2O loss during exhumation. The relatively low density of these brine FI (i.e. large vapor/liquid ratios; Fig. 1a and c) seems to support a retrograde FI dehydration trend.

FLUIDS IN DEEP SUBDUCTION ZONES

Chemical composition of fluids released during deep subduction

H*P* and UH*P* fluids released during subduction have a profound petrological and geochemical action both in the control of some state variables (first of all P_{H2O}), and in the dissolution and transport of chemical components from the slab by inducing metasomatic addition to the mantle wedge. Diverse fluid compositions are preserved in prograde and peak metamorphic phases of deeply subducted rocks: water-dominated C-O-H-N mixtures (e.g. Klemd 1989; 2013; Giaramita and Sorensen 1994; Vallis and Scambelluri 1996; El-Shazly and Sisson 1999; Franz et al. 2001; Gao and Klemd 2001), brines, N_2-CO_2/CH_4 fluids (e.g., Andersen et al. 1989; Selverstone et al. 1992; Philippot 1993; Klemd et al. 1992, 1995; Scambelluri et al. 1997, 1998; Xiao et al. 2000, 2002; Fu et al. 2001, 2002, 2003; Mukherjee

and Sachan 2009), aluminosilicate-rich aqueous fluid phases (e.g., Ferrando et al. 2005 and references cited), and, more rarely, hydrous melts.

Early studies by Philippot et al. (1995) first described a relevant variation in the chemistry of fluids passing from prograde H*P* to peak UH*P* metamorphic conditions in coesite-pyrope-bearing whiteschists from the Dora-Maira massif (Italian Western Alps). They noted that large quantities of dehydration fluids released during prograde metamorphism - predating pyrope and coesite UH*P* assemblage - were preserved as low-solute aqueous FI in relic kyanite within pyrope. Further evidence for dehydration fluids at UH*P* conditions, attending the growth of garnet, was given by MSI in pyrope, which contain phyllosilicates, Mg-phosphate, chlorides, and opaques, but no optically-visible aqueous fluid. Over time, fluid inclusion research combined with petrological investigations further demonstrated that water-rich fluids with variable halide contents (± N_2 and CH_4/CO_2) generally dominate in H*P* prograde, low-*T* UH*P* peak, and early retrograde metamorphic mineral assemblages, whereas complex aluminosilicate-rich aqueous fluid phases are typically preserved in UH*P* peak metamorphic mineral assemblages at *T* above about 600-650°C.

In the following sections, we provide a synthesis of the current knowledge on the chemical composition of fluids in deep subduction zones, based on fluid inclusion literature summarized in Table 1. We concentrate on those eclogite-facies rocks of crustal origin equilibrated at *P-T* conditions relevant for slabs at sub-arc depths (i.e., coesite facies; 2.5-4 GPa).

Aqueous fluids ± N_2

In some eclogite-facies rocks from Caledonian, Hercynian, and Alpine L*T*-H*P,* and -UH*P* metamorphic terranes, the prograde, peak, and early retrograde fluid composition within different rock types is uniform in terms of H_2O, which represents the main component, but

variable in terms of solutes, and non-polar components (N_2 contaminated by CO_2, or CH_4), as previously summarized by Scambelluri and Philippot (2001), Touret and Frezzotti (2003), Heinrich (2007), and Klemd (2013).

FI studies in eclogites from the Alps indicate that prograde aqueous fluids contain mainly NaCl and $MgCl_2$, with only subordinate concentrations of $CaCl_2$ and KCl. Calculated salinities vary from about 3 to 50 in NaCl equivalent wt. % (e.g., Philippot and Selverstone 1991; Selverstone et al. 1992; Philippot et al. 1995; Scambelluri et al. 2001). To explain the Na-, and Mg-dominated nature of such H*P* chloride-bearing solutions, two processes have been proposed: recycling of sea-water (Scambelluri et al. 1997), or hydrothermal alteration of the oceanic lithosphere (Philippot et al. 1998). More recently, Sharp and Barnes (2004) presented a model for the generation of mobile high-$MgCl_2$ aqueous plumes at mantle depths, via breakdown of subducted serpentinites.

In the Dabie-Shan and Sulu UH*P* eclogite-facies continental rocks, prograde and early retrograde metamorphic fluids preserved within FI are generally $CaCl_2$-dominated (Xiao et al. 2000, 2001; Fu et al. 2001, 2002, 2003; Zhang et al. 2005; Frezzotti et al. 2007), and not NaCl-rich as in oceanic rocks. Xiao et al. (2000) and Fu et al. (2001, 2003) reported also the presence of N_2, $\pm$ CO_2, or CH_4-rich H*P* fluids. In matrix rocks, the scale of fluid chemical heterogeneity is extremely variable. For example, in metasediments and eclogites from the Dabie-Shan UH*P* terrane, aqueous fluids have different salinities and, most importantly, different cations in solution, even at the scale of the crystal (Fu et al. 2002). In these fluids, the nature of cations is related to the host mineral phase (e.g. Ca-dominated chlorides in epidote, and Na-, K-chlorides in amphibole). Fluid chemical variability indicates very limited fluid transport before trapping as inclusions, and generally supports an internal origin. Based on the very low $\delta^{18}O$ of minerals containing FI in eclogite-facies continental rocks from Dabie-Sulu, Fu et al. (2002, 2003), Ferrando et al. (2005a), and Frezzotti et al. (2007)

proposed an ultimate origin from past meteoric water brought to mantle depths (e.g., Zhang et al. 2011, and references cited).

Besides chlorine and alkalis, additional minor solutes in aqueous fluids are Si, Al, Ti, C, and S species. The aluminosilicate content in aqueous fluids increases with increasing pressure, while chlorine shows the opposite trend. For example, prograde fluids formed at about 2.5 GPa and 600°C in the Dora-Maira whiteschists contain Cl, Mg, alkalis, with subordinate Si and Al (i.e., Na- and Mg-chlorides and paragonite as daughter phases in FI; Philippot et al. 1995; Ferrando et al. 2009). At 3.5 GPa and similar temperatures (600°C), peak aqueous fluids in UH*P* metasediments from Lago di Cignana, also in W Alps, contain dominantly Si, Al, Ti, C, Ca, and alkalis (e.g., quartz, rutile, paragonite, carbonate and diamond as daughter phases in FI; Frezzotti et al. 2011; 2014), while Cl appears as a very subordinate component.

From Table 1, calculated solute contents in FI range from less than 3 up to 50 wt. % in NaCl equivalent. Experiments and thermodynamic modeling suggest that aqueous fluids formed at depths below about 90 km are diluted solutions (< 20 wt. % in NaCl equivalent; e.g., Manning 1998; Kessel et al. 2005a; Hermann and Spandler 2008; Spandler and Picard 2013; and references cited). Considering that many H*P* aqueous fluids contain less than 30 wt. % solutes (cf., Table 1), most researchers have interpreted the inclusion fluid record to confirm a dominantly diluted nature of H*P* aqueous subduction-zone fluids. Fluid-fluid immiscibility processes (Newton and Manning 2010), or passive solute enrichment due to water loss from inclusions, could have brought to the extreme chloride enrichment observed in some FI.

H*P*-UH*P* FI highlight also the possible presence of non-polar fluid species, such as N_2, CO_2, and CH_4, although this last one is more commonly formed during early decompression (cf., Table 1; Xiao et al. 2000, 2002; Fu et al. 2001, 2002, 2003a, 2003b; Yang et al. 2001). N_2

372 is by far the most abundant non-polar gas in prograde and peak metamorphic fluids (cf.,
373 review by Touret 2001; Frezzotti and Touret 2003; Klemd, 2013). Up to 20 mole % N_2 were
374 measured in H*P* aqueous fluids in eclogites from western Norway, where eclogitization is
375 triggered by channeled fluids in shear zones (Austreheim 1987; Andersen et al. 1989; 1990;
376 1993). Although the thermodynamic properties of the C-O-H-N system are not fully known, it
377 is possible to trace the transition from H*P* to UH*P* conditions of aqueous fluids containing
378 nitrogen. Since the binary system H_2O - N_2 system shows a miscibility gap at P > 2-2.2 GPa
379 at temperatures ≤ 700°C (X_{N2} >0.2; Haefner et al. 2002), H_2O-N_2 fluids formed in the *P-T*
380 stability field of coesite are expected to be immiscible, while full H_2O-N_2 miscibility should
381 be expected at lower pressures.
382 N_2 fluids can form by release of ammonium (NH_4^+) substituting for K^+ in micas,
383 during prograde dehydration with increasing metamorphism (Hallam and Eugster 1976; Duit
384 et al. 1986; Haendel et al. 1986; Bebout and Fogel 1992; Bebout, 2013). The speciation of
385 nitrogen in C-O-H-N fluids depends on pressure, temperature, fluid composition, and is
386 probably controlled by redox conditions (Andersen et al. 1993; Pöter et al. 2004). It has been
387 shown, that, during cold subduction, almost the complete budget of nitrogen can remain in
388 micas up to 2.5 GPa (Busigny et al. 2003). In addition, boron nitride (BN) and osbornite
389 nitrides (TiN) inclusions in coesite have been reported at higher pressures (Dobrzhinetskaya
390 et al. 2008).
391
392 ***(Alkali) aluminosilicate-rich aqueous fluids***

393 MSI in UH*P* subduction rocks (P > 3GPa), formed at peak metamorphic temperatures
394 above about 600°C, typically consist of several hydrous (alkali) aluminosilicates, such as
395 paragonite, muscovite, chlorite, and phlogopite, and variable amounts of anhydrous and
396 hydrous sulfates, carbonates, phosphates, chlorides, and (former) H_2O (Table 1; Figs. 2, 3,
397 and 6). Over the last decade, the growing interest on these volatile-rich microsystems induced

to an increase of research and discussion to understand the composition and the properties of the fluid media that were originally trapped. From the compilation of data on daughter minerals in MSI, it is evident that Si, Al, and alkalis, but not halides, are the major constituents of UH*P* water-rich fluid phases preserved in MSI. Element solubility appears distinct from an aqueous fluid phase at crustal depths (cf., Yardley 2013). Deep subduction fluids contain far too much Al_2O_3 and SiO_2, which are known to have very limited solubility in water at crustal conditions, irrespective of salinity. Nonetheless, these water-rich phases have major element contents that do not resemble any silicate melts of magmatic composition, generated by volatile-saturated partial melting of metasedimentary or eclogitic rocks at high metamorphic grades.

A reconstruction of the major element composition of UH*P* water-rich phases has been attempted by Ferrando et al. (2005, 2009), and Frezzotti et al. (2007) averaging the vol. % of daughter minerals in MSI (EMPA analyses; for the procedure see Ferrando et al. 2005). The method suffers of uncertainties, in part due to the processes that may have affected inclusions during retrograde decompression, including chemical interaction with the host mineral phase (Heinrich and Gottschalk 1995; Svensen et al. 1999; Franz et al. 2001). Nevertheless, semi-quantitative analyses are sufficient for petrological investigations and provide constrains on the major element composition of water-rich phase released during deep subduction.

There is an evident link between the nature of chemical species present in UH*P* fluids and the chemistry of the matrix metamorphic rocks which undergo progressive devolatilization reactions. A nice example is represented by the composition of inclusion fluids in UH*P* eclogite-facies metamorphic series from the Sulu terrane, which consist of both sedimentary and igneous lithologies attaining the same *P-T* conditions (3.5 GPa, 750 °C). In UH*P* quartzite (phengite and epidote *s.l.* not stable) reconstructed peak fluid compositions indicate major SiO_2 (24 wt.%), Al_2O_3 (30 wt.%), CaO (9 wt.%), K_2O (5 wt.%), Na_2O (3

423 wt.%), and SO_3 (11 wt.%), with subordinate TiO_2, Fe_2O_3, FeO, MgO, BaO, P_2O_5, Cl^-, F, and
424 $(CO_3)^{2-}$. In eclogites, fluids have similar SiO_2 (26 wt.%), Al_2O_3 (20 wt.%), and CaO (7 wt.%),
425 but considerably higher MgO (4 wt.%), $FeO_{(tot)}$ (FeO = 6 wt.% Fe_2O_3= 4 wt.%), and P_2O_5,
426 and almost no alkalis, carbonates, and sulfates. More evidence supporting that UH*P* aqueous
427 phases can dissolve rock components can be found in the chemistry of fluids formed during
428 the growth of the large pyropes in Dora-Maira metasomatic whiteschists (phlogopite and talc
429 not stable; phengite stable; 4 GPa, 700 °C), which contain high MgO (25.5 wt%), SiO_2 (29
430 wt%), and Al_2O_3 (23 wt%), while extremely subordinate Fe_2O_3 (4.7 wt%), S (3.2 wt%), Na_2O
431 (1.3 wt%), CaO (0.6 wt%), P_2O_5 (0.4wt%), and K_2O (0.2 wt%).

432 A minimum water content of about 20 wt. % has been calculated considering the
433 amount of water bonded in daughter hydrous minerals in MSI, and hypothesizing that the void
434 volume between different daughter phases originally contained H_2O with a density of 1.3
435 g/cm^3 (cf., Ferrando et al. 2005 and references cited; Fig. 2, 3, 8, and 9). The original water
436 content of deep subduction fluids, however, should have been considerably higher, perhaps in
437 the order of 40-60 wt. %, in part lost by passive H_2O diffusion from inclusions during
438 retrogression. Chlorine contents are low, below a few unit wt. %, and CO_2, N_2 and CH_4 have
439 not been detected (e.g., Raman spectroscopy analyses).

440 Extending the examples discussed above with literature data in Table 1 shows that
441 progressive devolatilization reactions in rocks control the chemistry of aqueous fluids released
442 during deep subduction, depending on rock composition and *P-T* subduction path, as
443 predicted by theoretical and experimental petrology (e.g., Schmidt and Poli 1998, 2003;
444 Hermann 2002a; Hacker et al. 2003; Hermann et al. 2006). As illustrated in Figure 11, the
445 breakdown of phengite governs the alkali enrichment observed in alkali aluminosilicate
446 aqueous fluid phases in Sulu metasediments, while the Mg-enriched nature of Dora-Maira

447 UH*P* fluids derives from phlogopite and talc breakdown in these metasomatic rocks of crustal
448 origin.

449 In summary, the emerging feature from FI and MSI studies (Table 1) is that at H*P*
450 conditions, subduction zone fluids are relatively diluted aqueous solutions (± non-polar
451 gases), containing chlorides, alkalis, Si, and Al, with properties similar to crustal aqueous
452 fluids. At greater sub-arc depths, fluids released by crustal lithologies contain increasing
453 amounts of alkali aluminosilicate components ± carbonates phosphates, and sulfates/sulfides,
454 while halides do not appear anymore more as the principal ligands. Thus, although we must
455 acknowledge the limitations of quantitative major element analyses in FI and MSI, observed
456 chemical variations provide key insights into element solubility in deep-subduction aqueous
457 fluids, which results from major structural variations, as it will be discussed in the next
458 section.

459

460 **Experimental approach: Structure and solvent capacity of H*P*/UH*P* fluids**

461 Knowledge of deep subduction-zone fluids behavior implicitly demands for
462 thermodynamic models. When considering the chemical composition of FI and MSI, it is
463 clear that water is the relevant volatile at sub-arc depths. However, water-rich phases
464 containing a great silicate concentration (i.e., MSI) have properties which are intermediate
465 between those generally attributed to aqueous fluids and to hydrous silicate melts, an obvious
466 avenue for experiments and theoretical models.

467 Experimental and theoretical studies on quartz solubility in water have shown that at
468 high pressure, the silica content of aqueous fluids rises considerably, and the silica-saturated
469 fluid phase and the water-saturated melt progressively approach each other (Fig. 12; Newton
470 & Manning 2008; Mysen 2010; Dolejš and Manning 2010; Hunt and Manning 2012). In the

SiO_2-H_2O system, immiscibility between melt and fluid vanishes at the upper critical endpoint (point C in Fig. 12), as aqueous fluids form a single continuous solution with silicate melts (Kennedy et al. 1962; Anderson and Burnham 1965; Paillat et al. 1992; Ryabchikov 1993; Bureau and Keppler 1999; Newton and Manning, 2008; Stalder et al. 2000, 2001). The *P-T* location of the upper critical endpoint for the SiO_2-H_2O system was determined at 1 GPa and 1080°C by Kennedy et al. (1962) and Anderson and Burnham (1965). In natural systems, the *P-T* conditions of the upper critical endpoint depend on the chemistry of the silicate system. For example, they correspond to 2 GPa and 700 °C for the NaAl-Si_3O_8–H_2O system (Paillat et al. 1992; Stalder et al. 2000). For more complex systems, such as basalt-H_2O, Ca-bearing granite-H_2O, haplogranite-H_2O, jadeite-H_2O, nepheline-H_2O, supercritical *P-T* conditions have been proposed at pressures variable from 3.4 to 6.0 GPa, with currently no general consensus (for discussion cf., Eggler and Rosenhauer 1978; Ryabchikov 1993; Bureau and Keppler 1999; Mysen and Shang 2003; Mibe et al. 2011).

Based on thermodynamics, the nature of UH*P* fluids in subduction zones has been discussed at great length in the literature, and several definitions have been applied: intermediate fluids (Manning 2004; Frezzotti et al. 2007; Ferrando et al. 2009), supercritical liquids (Schmidt et al. 2004; Kessel et al. 2005b; Mysen 2012; Spandler and Pirard 2013), supercritical fluids (Ferrando et al. 2005a; Malaspina et al. 2006; Hack et al. 2007a; Liebscher 2010; Zhang et al. 2011; Zheng et al. 2011; Kawamoto et al. 2012), supercritical hydrous melts and transitional fluids (Hermann et al. 2006, 2013). Recently, Sanchez-Valle (2013) proposed to adopt the term *fluid* for any water-rich phases released in subduction zones at sub-arc depths, since: *"the meaningful distinction of liquid, vapor, gases at ambient conditions becomes obsolete at high pressures and temperatures where transitions between the various fluid types are often gradational"*.

At high pressure and temperature conditions, the (supercritical) fluid vs. melt *vexata quaestio* is more a semantic than a petrological controversy. As summarized by Hack et al. (2007b) most subduction geothermal gradients are likely to reach *P*-*T* conditions close or above the upper critical endpoints of most crustal lithologies. Thus, during deep subduction, the hydrous *solidus* should be seen as a convenient temperature boundary at which the concentration of silicate components dissolved into aqueous fluids progressively increases, without the abrupt chemical changes resulting at crustal *P*-*T* conditions (cf., Fig. 11).

FI and MSI demonstrate beyond reasonable doubt the relevant and gradual increase of the (alkali) aluminosilicate solute load, without phase change, predicted in model fluids by thermodynamics at increasing *P* (Fig. 12; e.g., Bureau and Keppler 1999; Hunt and Manning 2012). For example, at depths greater than about 90-100 km *(P* ≥ 3.2 GPa) with transport to UH*P* conditions with little concomitant heating (*T*=600°C), water dominates over alkali aluminosilicate solutes in released fluids (Fig. 12; FI in UH*P* rocks from Alps). At higher *P* and sub-magmatic temperatures (*P* = 3.4-4 GPa; *T* = 700-800°C), approaching the hydrous *solidus* for sedimentary and granitic rocks, aqueous fluids record an increase of solubility of Si, Al, and alkalis by at least a factor of ten, reaching about 50-60 wt. % solutes (Fig. 12; MSI in UHP rocks from Alps and Dabie Shan-Sulu). Fluids released at extremely high *P* and *T* (about 5-8 GPa, and 900°C; Kokchetav Massif; Dobrzhinetskaya et al. 2003a; Hwang et al. 2006; Korsakov and Hermann 2006; Hermann et al. 2013) consist mostly of aluminosilicate components, appearing as hydrous silicate melts. This last case, however, applies to very deep subduction, probably not directly reflecting on arc magma generation.

Enhanced silicate solubility approaching critical "mixing" of silicate-aqueous fluids is due to solute structure change from (hydrated) ions to monomers and higher polymers (Newton and Manning 2002; 2003; Hunt and Manning 2012). Silica polymerization was recognized in aqueous fluids by *in-situ* spectroscopic studies both from experiments at high

pressures (Zotov and Keppler 2002), and in FI in UH*P* metamorphic rocks (Fig. 13; Lago di Cignana metasediments). Although polymerized aqueous fluids can reach a state of hydration which is similar to that in hydrous silicate melts, their physical properties are different, perhaps more akin to that of colloidal silica (e.g., Iler 1979; Hunt and Manning 2012). In the albite-H_2O system (Fig. 14), UH*P* fluids containing up to about 60 wt. % solutes show considerably lower viscosities than hydrous melts, and form a linear trend towards pure water values (Hack and Thompson 2011). Higher polymeric complexes, with characteristics similar to hydrous melts, only form at much greater solute concentrations (well above 80 wt. %; Hack and Thompson 2011).

Based on these observations, it appears not convenient to distinguish UH*P* aqueous fluid phases in terms of various categories based on the solute (e.g., SiO_2) load (e.g., supercritical fluids or supercritical melts). Across the *P-T* range of most subduction zones, silicate solubility can increase multifold in polymerized fluids, as well as the amount of carbonate and sulfide/sulfate complexes, resulting in variable fluid densities and viscosities. Polymerization at high pressure softens the transition from *sub-solidus* to *super-solidus* conditions that governs the volatile behavior at shallower crustal conditions. These properties directly reflect on the rate of mass transfer into the mantle wedge, and suggest that deep aqueous fluids can represent effective metasomatic agents in the mantle wedge.

Element recycling by deep subduction fluids

Trace elements

To what extent the physico-chemical properties of UH*P* fluids, in particular ligand species and concentration, influence elements fractionation between aqueous fluids and matrix rocks during deep subduction directly reflects on metasomatism of the mantle wedge.

Element transfer by solute-poor aqueous fluids at depths of less than 90 km is generally considered very limited, and gives way to transfer via hydrous melts or polymerized aqueous fluids at sub-arc depths (see e.g., Manning 2004; Kawamoto 2006; Spandler et al. 2007; Hermann and Spandler 2008; and references cited). At depths greater than about 90 km, sedimentary, and oceanic rocks in the slab are expected to have different amounts of the same minerals, and at *T* of about 750-800°C, they would initiate melting if water-saturated (Schmidt et al. 2004). According to several authors (e.g., Johnson and Plank 1999; Rudnick et al. 2000; Hermann and Rubatto 2009), incipient hydrous melting of slab rocks represents the most important source of incompatible elements into the overlying mantle wedge. The LILE-enriched, HFSE (Ti, Zr, Hf, Nb, Ta) depleted incompatible element pattern of arc-magma would result from dissolution of mineral phases, such as phengite (LILE, and Be; e.g., Schmidt and Poli 1998, 2003; Hermann et al. 2006; Hermann and Spandler 2008), epidote (REE, Sr, Th, Pb; e.g., Schmidt and Poli 1998, 2003; Hermann 2002a; Hermann et al. 2006), lawsonite (REE, Sr, Pb, Th, U; e.g., Martin et al. 2011), allanite/monazite (La, Ce, Th; e.g., Hermann 2002b; Hermann and Rubatto 2009), leaving in the residue refractory zircon (Zr, Hf), and rutile (Ti, Nb, Ta).

Kessel et al. (2005b) investigated the fluid/rock and melt/rock partition coefficients of trace elements for water-saturated K-free synthetic basaltic systems from 4 to 6 GPa and from 700° to 1200°C. Their experimental data suggested that trace element fractionation resembles subduction patterns in arc magmas, showing enrichments in LREE, LILE, Th, U, and Pb, and depletion in HFSE. Differences in the partitioning behavior of trace elements diminish with increasing depth and temperature, and at high *P*-*T* conditions, the trace element load of aqueous fluids and hydrous melts becomes increasingly alike, and varies continuously with temperature.

568 Data on the trace element concentrations of natural UH*P* fluids have been reported
569 only by a small number of examples, mainly because of the difficulties in analyzing MSI. In
570 these studies (Fig. 15), quantitative element concentrations in MSI were obtained by Laser
571 Ablation-Inductively Coupled Plasma-Mass Spectrometer (LA-ICP-MS) in rehomogenized
572 (for the method, see Malaspina et al. 2006), and in unheated inclusions (for the method, see
573 Halter et al. 2002), using Ca and/or Si as internal standards. Malaspina et al. (2006, 2009)
574 reported the first trace element data for MSI in metasomatic garnet meta-orthopyroxenite (P =
575 4 GPa, T = 750 °C) from the Maowu Complex in the Dabie Shan. UH*P* fluid trace element
576 patterns show fractionations similar to arc magmas, with LILE (Cs, Pb, Rb, Sr, Ba), LREE, U,
577 Pb, Th (high U/Th) enrichments, and HFSE (Ti, Zr, Hf, Nb, Ta) depletion (Fig. 15a). They
578 suggested that metasomatic fluids leading to important orthopyroxene and garnet
579 crystallization in peridotites were solute-rich aqueous fluids derived from surrounding crustal
580 lithologies.

581 In deeply-subducted crustal rocks, the geochemical signature of UH*P* fluids was
582 investigated by Ferrando et al. (2009) in the Dora-Maira whiteschists, formed by metasomatic
583 processes during prograde H*P* evolution. Magnesium-rich aluminosilicate aqueous fluids,
584 released during the growth of peak garnet (about 4 GPa and 750°C), are enriched in trace
585 elements compared to the whiteschists (Fig. 15b), and contain fractionated incompatible trace
586 element patterns with positive spikes for LILE, U, and Pb (up to about 100 to 1000 times the
587 mantle; Fig. 15b), and negative HFSE anomalies (Ti, Zr, Nb, Ta). Although some LILE reach
588 "granitic" melt concentrations, element fractionation in fluids does not strictly reflect either an
589 aqueous fluid (i.e., low Ba/Cs, Rb/Cs), or a silicate melt (low LREE, Sr, and Th enrichment
590 trend). Measured LILE enrichments, over LREE and HFSE, are in agreement with a main
591 contribution from the breakdown of phlogopite. Most of the released Rb, Ba and Th, however,
592 remain in phengite, which represents the stable mica at peak metamorphic conditions (Fig.

15b). Accessory monazite, Mg-dumortierite, zircon, and rutile in matrix whiteschists control the HFSE and LREE rock budget (Fig. 15b).

Geochemical data like those of the two examples discussed above are extremely valuable, since preserve an experimental flavor, reflecting the chemical control imposed by the metamorphic evolution of rocks. There is an interesting parallel between experimentally-derived fluid-mineral partitioning data which predict enhanced incompatible trace element solubility in UH*P* fluids at, or close to supercritical conditions (Kessel et al. 2005b), and the capacity of natural fluids to selectively extract LILE and LREE during prograde metamorphism (from H*P* to UH*P* conditions). In deep subduction fluids, incompatible element upload is enhanced by mineral dissolution, but governed by metamorphic reactions.

Comparison between examples from the literature further allows us to evaluate the extent of LILE/HFSE fractionation by deep slab fluids. Rutile is a common daughter phase in many FI and MSI (Table 1), pointing to mobilization of HFSE in polymerized fluids. Interestingly, relevant TiO_2 concentrations are observed also in dilute UH*P* aqueous fluids formed at relatively low *T*, provided that they contain alkalis (cf., Table 1). The efficiency of HFSE uptake appears mainly controlled by fluid properties at high *P*, and directly associated with the matrix slab-rock chemical composition. A similar geochemical behavior is different to that proposed for mass transfer by hydrous silicate melts, where the concentration of HFSE has been recognized to be fundamentally a function of the degree of melting (cf., Hermann and Rubatto 2009, and references cited): in other words, it is temperature dependent. Accessory minerals controlling the HFSE budget of slab-rocks have been experimentally found to be stable up to 850-900 °C.

Thus, alkali aluminosilicate fluids in subduction zones can mobilize and transport HFSE, also at *sub-solidus* thermal conditions. This is in accordance with experimental and thermodynamic research (e.g., Antignano and Manning 2008; Manning et al. 2008; Wilke et

al. 2012; Sanchez-Valle 2013), and with extensive field evidence (e.g., Selverstone et al. 1992; Rubatto and Hermann 2003; Garrido et al. 2005; Gao et al. 2007). However, HFSE should be lost by UH*P* fluids during transport into the mantle wedge, before reaching the hotter levels where subduction magmas are generated. According to Garrido et al. (2005) chlorite-bearing peridotites overlying subducting slab could represent the potential HFSE filters removing these elements from slab fluids, without changing their LILE budget. Only after metasomatic re-equilibration, fluids would acquire the LILE-enriched and HFSE-depleted trace element pattern characterizing arc magma.

Carbon

A major issue of subduction-zone geochemistry is to model and quantify the fluxes of volatiles released into the mantle wedge, and returned to the exosphere via arc magmatism. Carbon isotopic composition in volcanic gases of arc magmas requires that most of the Earth's degassed CO_2 is recycled (e.g., Alt and Teagle 1999), suggesting that fluids released from the subducting slab metasomatically enrich in carbon the mantle wedge. Modeling the fluxes of carbon ingassing is, however, difficult, since release of carbon during subduction is modeled as a discontinuous process.

In slab rocks, carbon is present in a variety of forms, including carbonate minerals and organic matter, derived from altered oceanic crust and marine sediments. Part of the carbon originally present in crustal lithologies is liberated as CO_2, during low-grade metamorphic decarbonation reactions (e.g., Kerrick and Connolly 2001), or fixed as graphite (Foustoukos 2012; Galvez et al. 2013). At greater sub-arc depths, coupled thermal and thermodynamic models strongly suggest that carbonate minerals do not react with silicate phases liberating CO_2, and are stable along most subduction geothermal gradients (Connolly 2005; Gorman et al. 2006;

642 Molina and Poli 2008). In the absence of carbonate melting, most subducted carbon is predicted
643 to be transported deep in the mantle (Dasgupta et al. 2004; Poli et al. 2009).

644 Fluid inclusions in eclogites-facies rocks have been generally used to support the models,
645 as they contain little to no detectable CO_2, in contrast to fluid inclusions in many other
646 metamorphic environments (e.g., granulites; Touret 2001). Limiting the carbon inventory within
647 FI and MSI to the absence of CO_2, however, can result in an underestimation of the carbon
648 budget in UH*P* fluids. Carbonates have been reported in FI and MSI from several UH*P* terranes,
649 often associated with microdiamonds (cf., Table 1; and Dobrzhinetskaya 2012). For example,
650 Dobrzhinetskaya et al. (2007) identified H_2O molecules and carbonate ions in nanometric MSI in
651 Erzgebirge diamonds; Korsakov and Hermann (2006) described carbonate-rich MSI in diamond-
652 bearing calc-silicate rocks from Kokchetav massif. Crystallization from supercritical C-O-H
653 fluids represents the current preferred mechanism by most researchers to account for subduction
654 (i.e., metamorphic) diamond formation (cf., Dobrzhinetskaya 2012; and references cited).
655 Precipitation of diamond from C-O-H fluids containing carbonate ions, among other species,
656 implies that high f_{O2} are prevailing in fluid phases (e.g., CCO buffer, Dobrzhinetskaya et al.
657 2001; de Corte et al. 2002). Yet, most diamond-bearing UH*P* metamorphic rocks record *P*-*T*
658 conditions (4-8 GPa, and 950-1000°C) that greatly exceed those of arc magma genesis, and
659 hence involve transport of carbon that cannot follow a simple return trajectory to the surface
660 through arc magmatism.

661 Spectroscopic study of carbon speciation in FI from oceanic-crust metasediments from
662 Lago di Cignana in western Alps shed light on the mechanisms of carbon liberation and transport
663 by deep subduction fluids at *P*-*T* conditions directly relevant to slab-mantle-arc transfer ($P \geq 3.2$
664 GPa; T = 600°C). Raman analyses of C species in aqueous FI formed about 100 km depth,
665 revealed appreciable amounts of oxidized carbon dissolved as CO_3^{2-}(aq) and HCO_3^-(aq), along
666 with hydrous and hydrated carbonates and diamond, and no detectable CO_2 (Fig. 13b; Frezzotti

et al. 2011; 2014). These results strongly suggest that dissolution of carbonate minerals in aqueous fluids as carbonate ions, in addition or alternatively to decarbonation, is a relevant process for carbon transfer into the mantle wedge during subduction. Further, FI data indicate a major role of water in the transport of carbon at *P-T* conditions that are directly relevant to slab-mantle-arc transfer, with implications for the Earth's carbon cycle.

Recent geochemical, experimental, and theoretical research suggest similar trends for the release and transport of oxidized carbon during deep subduction (cf., Manning et al. 2013; and references cited). Ague and Nicolescu (2014) proposed that carbonate dissolution, accompanied by silicate precipitation, represents a relevant mechanism for the release of oxidized carbon from subduction zones, based on carbonate $\delta^{18}O$ and $\delta^{13}C$ systematics, combined with rock and fluid inclusion studies in metamorphic rocks from the Cycladic complex. By computing the dielectric constant of water at upper mantle *P-T* conditions, Pan et al. (2013) predicted the solubility of carbonate minerals in the subducting lithosphere during dehydration reactions. Similar results were obtained by spectroscopy experiments by Sanchez-Valle et al. (2013), which identified carbonate ions as the dominant C-species in oxidized UH*P* aqueous fluids at *P-T* conditions (650°C and 4 GPa) similar to those of Lago di Cignana rocks. The results summarized above illustrate that investigations on the deep Earth's carbon cycle have entered a new phase where observations in natural rock systems, thermodynamic models, and experimental research can be merged. New research modifies the magnitude of carbon fluxes in the mantle in subduction zones, and points to a strong need for a better quantification of the properties of carbon species and minerals at depth.

IMPLICATIONS

Present review shows that fluid inclusions (FI and MSI) are almost ubiquitous in eclogite-facies crustal lithologies of both continental and oceanic origin. Their composition appears to be controlled by the progressive devolatilization reactions occurring in rocks at H*P* and UH*P* conditions, thus preserving a firsthand information on deep subduction fluids.

Water is the dominant volatile species in subduction-zone fluids, which contain variable concentration of solutes, and of other volatiles. At H*P* conditions down to about 90 km depth (i.e., fore-arc), moderate concentrations of chloride salts, alkalis, Si, and Al , ± non-polar gases are present in aqueous solutions, with properties similar to crustal fluids (e.g., halide ligands); at greater mantle depths (i.e., sub-arc), water-rich phases contain gradually increasing amounts of (alkali) aluminosilicate components (e.g., Si, Al, Ca, Fe, alkalis, Ti, Zr, $(SO_4)^{2-}$, $(CO_3)^{2-}$, and Cl^-). Inclusion fluids record the solute structure change from (hydrated) ions to monomers and higher polymers in aqueous fluids at increasing pressure during subduction.

Semi-quantitative chemical data on major and trace element enrichments in FI and MSI, together with experimental and thermodynamic research, unambiguously attest for relevant and selective element mobilization in UH*P* aqueous fluids, enhanced by mineral dissolution, and ruled by the composition of matrix rocks. Increased element solubility and transport by the aqueous phase is related to silica polymerization, as the pressure and temperature conditions approach the critical endpoint.

It must be emphasized that research on fluid inclusions suggests that deep subduction fluids have more complex chemical compositions than those of model fluids considered by experiments. The finding of substantial amounts of dissolved oxidized carbon in aqueous fluids at sub-arc depths implies a reconsideration of the petrological models supporting liberation of C

715 into the mantle wedge by metamorphic decarbonation reactions only, and to consider dissolution
716 and transport of carbon by aqueous fluids a relevant process in deep subduction zones.

717 Despite the amount of data so far obtained, open questions do remain. The chemical
718 behavior of other ligands, such as sulfur, is still very poorly constrained, although it is generally
719 acknowledged that slab-fluid transfer into the mantle wedge causes both oxidation and S
720 addition. Fluid inclusions could probably provide a most robust insight to the behavior of sulfur
721 species, by combining chemical and structural analyses. Analytical work should be undertaken to
722 reveal if the high solute load observed in some inclusions (for example MSI) is a primary
723 feature, or alternatively results in part from passive dehydration trends. A better quantification of
724 inclusions post-trapping chemical modifications, including element diffusion, and exchanges
725 with the host mineral, is also essential.

726 We believe that fluid inclusion research in subduction zones will provide exciting new
727 results in the coming years. Although hampered by many analytical difficulties, the study of
728 fluids in rocks provides the added value of revealing the continuity existing behind the apparent
729 extreme variations of the physico-chemical properties of aqueous fluids progressively released
730 during deep subduction.

731

732 **ACKNOWLEDGEMENTS**

733 We are grateful to D. Foustoukos for inviting us to write this contribution, and for his
734 efficient editorial handling. We thank J. Touret and an anonymous reviewer for their comments
735 that greatly improved the manuscript. We thank N. Malaspina and B. Stöckhert for providing
736 nice illustrations of their research. This study was in part supported by Italian PRIN grant
737 2010PMKZX7 to MLF.

738

REFERENCES

Ague, J.J., and Nicolescu, S. (2014) Carbon dioxide released from subduction zones by fluid-mediated reactions. Nature Geoscience 7, 355–360 doi:10.1038/ngeo2143

Alt, J.C., and Teagle, A.H. (1999) Uptake of carbon during alteration of oceanic crust. Geochimica et Cosmochimica Acta, 63, 1527-1535.

Andersen, T., Burke, E.A.J., and Austrheim, H. (1989) Nitrogen-bearing, aqueous fluid inclusions in some eclogites from the Western Gneiss Region of the Norvegian Caledonides. Contributions to Mineralogy and Petrology, 103, 153-165.

Andersen, T., Austrheim, H., and Burke, E.A.J. (1990) Fluid inclusions in granulites and eclogites from the Bergen Arcs, Caledonides of W. Norway. Mineralogical Magazine, 54, 145-158.

Andersen, T., Austrheim, H., and Burke, E.A.J. (1993) N_2 and CO_2 in deep crustal fluids: evidence from the Caledonides of Norway. Chemical Geology, 108, 113-132.

Anderson, G.M., and Burnham, C.W. (1965) The solubility of quartz in supercritical water. American Journal of Science, 263, 494-511.

Angiboust, S., Langdon, R., Agard, P., Waters, D., and Chopin, C. (2012) Eclogitization of the Monviso ophiolite (W. Alps) and implications on subduction dynamics. Journal of Metamorphic Geology, 30, 37-61.

Antignano, A., and Manning, C.E. (2008) Rutile solubility in H_2O, H_2O-SiO_2, and H_2O-$NaAlSi_3O_8$ fluids at 0.7-2.0 GPa and 700-1000 degree C: implications for mobility of nominally insoluble elements. Chemical Geology, 255, 283-293.

Austrheim, H. (1987) Eclogitization of lower crustal granulites by fluid migration through shear zones. Earth and Planetary Science Letters, 81, 221-232.

Bebout, G.E. (2007) Metamorphic chemical geodynamics of subduction zones. Earth and Planetary Science Letters, 260, 373-393.

Bebout, G.E. (2013) Metasomatism in Subduction Zones of Subducted Oceanic Slabs, Mantle Wedges, and the Slab-Mantle Interface. The role of fluids in Terrestrial and extraterrestrial processes. In D.E. Harlow, and H. Austrheim, Eds. Metasomatism and the Chemical Transformation of Rock, p. 289-350. Springer-Verlag, Berlin Heidelberg.

Bebout, G.E., and Fogel, M.L. (1992) Nitrogen-isotope compositions of metasedimentary rocks in the Catalina Schist, California: implications for metamorphic devolatilization history. Geochimica et Cosmochimica Acta, 56, 2139-2149.

Bureau, H., and Keppler, H. (1999) Complete miscibility between silicate melts and hydrous fluids in the upper mantle: experimental evidence and geochemical implications. Earth and Planetary Science Letters, 165, 187-196.

773 Busigny, V., Cartigny, P., Philippot, P., Ader, M., and Javoy, M. (2003) Massive recycling of
774 nitrogen and other fluid-mobile elements (K, Rb, Cs, H) in a cold slab environment: evidence from
775 HP to UHP oceanic metasediments of the Schistes Lustrés nappe (western Alps, Europe). Earth and
776 Planetary Science Letters, 215, 27-42.

777 Carswell, D.A., and Compagnoni, R. (2003) Introduction with review of the definition, distribution
778 and geotectonic significance of ultrahigh pressure metamorphism. In D.A. Carswell, and R.
779 Compagnoni, Eds. Ultrahigh-pressure metamorphism. E.M.U. Notes in Mineralogy, 5, p. 3-10.

780 Carswell, D.A., and Van Roermund, H.L.M. (2005) On multi-phase mineral inclusions associated
781 with microdiamond formation in mantle-derived peridotite lens at Bardane on Fiørtoft, west
782 Norway. European Journal of Mineralogy, 17, 31-42.

783 Castelli, D., Rolfo, F., Groppo, C., and Compagnoni, R. (2007) Impure marbles from the UHP
784 Brossasco-Isasca Unit (Dora-Maira Massif, western Alps): evidence for Alpine equilibration in the
785 diamond stability field and evaluation of the $X(CO_2)$ fluid evolution. Journal of Metamorphic
786 Geology, 25, 587-603.

787 Cesare, B., Ferrero, S., Savioli-Mariani, E., Pedron, D., and Cavallo, A. (2009) "Nanogranite" and
788 glassy inclusions: the anatectic melt in migmatites and granulites. Geology, 37, 627-630.

789 Connolly, J.A.D. (2005) Computation of phase equilibria by linear programming: a tool for
790 geodynamic modeling and its application to subduction zone decarbonation. Earth and Planetary
791 Science Letters, 236, 524-541.

792 Dasgupta, R., Hirschmann, M.M., and Dellas, N. (2005) The effect of bulk composition on the
793 solidus of carbonated eclogite from partial melting experiments at 3 GPa. Contributions to
794 Mineralogy and Petrology, 149, 288-305.

795 De Corte, K., Cartigny, P., Shatsky, V.S., Sobolev, S.V., and Javoy, M. (1998) Evidence of fluid
796 inclusions in metamorphic microdiamonds from the Kokchetav massif, northern Kazakhstan. .
797 Geochimica et Cosmochimica Acta, 62, 3765-3773.

798 De Corte, K., Taylor, W.R., and De Paepe, P. (2002) Inclusion contents of microdiamonds from
799 UH*P* metamorphic rocks of the Kokchetav massif. In: C.D. Parkinson, I. Katayma, J.G. Liou, and
800 S. Maryama, Eds., The Diamond-Bearing Kokchetav Massif, Kazakhstan. Universal Academy
801 Press, Inc., Tokyo, Japan, p. 115–135.

802 Dobrzhinetskaya, L.F. (2012) Microdiamonds — Frontier of ultrahigh-pressure metamorphism: A
803 review. Gondwana Research 21, 207-223.

804 Dobrzhinetskaya, L.F., Green, H.W., Mitchell, T.E., and Dickerson, R.M. (2001) Metamorphic
805 diamonds: mechanism of growth and oxides inclusions. Geology, 29, 253-266.

806 Dobrzhinetskaya, L.F., Green, H.W., Bozhilov, N.K., Mitchell, T.E., and Dickerson, R.M. (2003a)
807 Crystallization environment of Kazakhstan microdiamond: evidence from nanometric inclusions
808 and mineral associations. Journal of Metamorphic Geology 21, 425-437.

Dobrzhinetskaya, L.F., Green, H.W., Weschler, M., Darus, M., Wang, H.J., Massonne, H.J., and Stöckhert, B. (2003b) Focused ion beam technique and transmission electron microscope studies of microdiamonds from the Saxonian Erzebirge, Germany. Earth and Planetary Science Letters, 210, 399-410.

Dobrzhinetskaya, L.F., Wirth, R., and Green, H.W. (2007) A look inside of diamond-forming media in deep subduction zones. Proceedings of the National Academy of Sciences of the United States of America, 104, 9128–9132.

Dobrzhinetskaya, L., Wirth, R., Yang, J., Green, H., Weber, P., and Hutcheon, I. (2008) Boron and Nitrogen in ultrahigh-pressure terrestrial rocks. Geochimica et Cosmochimica Acta, 72, A221.

Dobrzhinetskaya, L.F., Wirth, R., Green, H.W., Schreiber, A., and Obannon, E. (2012) First find of polycrystalline diamond in ultrahigh-pressure metamorphic terrane of Erzgebirge, Germany. Journal of Metamorphic Geology, 31, 5-18.

Dolejš, D., and Manning, C.E. (2010) Thermodynamic model for mineral solubility in aqueous fluids: theroy, calibration and application to model fluid-flow systems. Geofluids, 10, 20-40.

Duit, W., Jansen, J.B.H., Breeman, A.V., and Bos, A. (1986) A mmonium micas in metamorphic rocks as exemplified by Dome de I'Agout (France). American Journal of Science, 286, 702-732.

Eggler, D.H., and Rosenhauer, M. (1978) CO_2 in silicate melts: II. Solubilities of CO_2 and H_2O in $CaMgSi_2O_6$ (diopside) liquids and vapours at pressures to 40 kbar. American Journal of Science, 278, 64-94.

El-Shazly, A.K., and Sisson, V.B. (1999) Retrograde evolution of eclogites and blueschists from NE Oman: evidence from fluid inclusions and petrological data. Chemical Geology, 154, 193-223.

Ferrando, S., Frezzotti, M.L., Dallai, L., and Compagnoni, R. (2005a) Fluid-rock interaction in UHP phengite-kyanite-epidote eclogite from the Sulu orogen, Eastern China. International Geology Review, 47, 750-774.

Ferrando, S., Frezzotti, M.L., Dallai, L., and Compagnoni, R. (2005b) Multiphase solid inclusions in UHP rocks (Su-Lu, China): remnants of supercritical silicate-rich aqueous fluids released during continental subduction. Chemical Geology, 223, 68-81.

Ferrando, S., Frezzotti, M.L., Petrelli, M., and Compagnoni, R. (2009) Metasomatism of continental crust during subduction: the UHP whiteschists from the Southern Dora-Maira Massif (Italian Western Alps). Journal of Metamorphic Geology, 27, 739-756.

Foustoukos, D.I. (2012) Metastable equilibrium in the C-H-O system: Graphite deposition in crustal fluids. American Mineralogist, 97, 1373-1380.

Franz, L., Romer, R.L., Klemd, R., Schmid, R., Oberhänsli, R., Wagner, T., and Dong, S. (2001) Eclogite-facies quartz veins within metabasites of the Dabie Shan (eastern China): pressure-temperature-time-deformation path, composition of the fluid phase and fluid flow during exhumation of high-pressure rocks. Contributions to Mineralogy and Petrology, 141, 322-346.

Frezzotti, M.L. (1992) Magmatic immiscibility and fluid phase evolution in the Mount Genis granite (southeastern Sardinia, Italy). Geochimica et Cosmochimica Acta, 56, 21-33.

Frezzotti, M.L. (2001) Silicate-melt inclusions in magmatic rocks:applications to petrology. Lithos, 55, 273-299.

Frezzotti, M.L., and Ferrando, S. (2007) Multiphase solid inclusions in ultra-high pressure metamorphic rocks: a petrographic approach. Periodico di Mineralogia, 76, 113-125.

Frezzotti, M.L., Ferrando, S., Dallai, L., and Compagnoni, R. (2007) Intermediate alkali-alumino-silicate aqueous solutions released by deeply subducted continental crust: fluid evolution in UHP OH-rich topaz-kyanite quartzites from Donghai (Sulu, China). Journal of Petrology, 48, 1219-1241.

Frezzotti, M.L., Ferrando, S., Peccerillo, A., Petrelli, M., Tecce, F., and Perucchi, A. (2010) Chlorine-rich metasomatic H_2O–CO_2 fluids in amphibole-bearing peridotites from Injibara (Lake Tana region, Ethiopian plateau): nature and evolution of volatiles in the mantle of a region of continental flood basalts. Geochimica et Cosmochimica Acta 74, 3023–3039.

Frezzotti, M.L., Selverstone, J., Sharp, Z.D., and Compagnoni, R. (2011) Carbonate dissolution during subduction revealed by diamond-bearing rocks from the Alps. Nature Geoscience, 4, 703-706.

Frezzotti, M.L., Ferrando, S., Tecce, F., and Castelli, D. (2012a) Water content and nature of solutes in shallow-mantle fluids from fluid inclusions. Earth and Planetary Science Letters, 351-352, 70-83.

Frezzotti, M.L., Tecce, F., and Casagli, A. (2012b) Raman spectroscopy for fluid inclusion analysis. Journal of Geochemical Exploration, 112, 1-20.

Frezzotti, M.L., Huizenga, J.M., Compagnoni, R., and Selverstone, J. (2014) Diamond formation by carbon saturation in C–O–H fluids during cold subduction of oceanic lithosphere. Geochimica et Cosmochimica Acta, http://dx.doi.org/10.1016/j.gca.2013.12.022.

Fu, B. (2002) Fluid regime during high- and ultrahigh-pressure metamorphism in the Dabie-Sulu terranes, eastern China: a stable-isotope and fluid inclusion study., Unbuplishd Ph.D. Thesis, p. 144. Vrije Universiteit Amsterdam.

Fu, B., Touret, J.L.R., and Zheng, Y.F. (2001) Remnants of pre-metamorphic fluid and oxygen-isotopic signatures in eclogites and garnet clinopyroxenite from the Dabie-Sulu terranes, eastern China. Journal of Metamorphic Geology, 21, 561-578.

Fu, B., Zheng, Y.F., and Touret, J.L.R. (2002) Petrological, isotopic and fluid inclusion studies of eclogites from Sujiahe, NW Dabie Shan (China). Chemical Geology, 187, 107-128.

Fu, B., Touret, J.L.R., and Zheng, Y.F. (2003a) Remnants of pre-metamorphic fluid and oxygen-isotopic signatures in eclogites and garnet clinopyroxenite from the Dabie-Sulu terranes, eastern China. . Journal of Metamorphic Geology, 21, 561-578.

Fu, B., Touret, J.L.R., Zheng, Y.F., and Jahn, B.M. (2003b) Fluid inclusions in granulites, granulitized eclogites and garnet clinopyroxenites from the Dabie-Sulu terranes, eastern China. Lithos, 70, 293-319.

Galvez, M.E., Beyssac, O., Martinez, I., Benzerara, K., Chaduteau, C., Malvoisin, B., and Malavieille, J. (2013) Graphite formation by carbonate reduction during subduction. Nature Geoscience, 6, 473-377.

Gao, J., and Klemd, R. (2001) Primary fluids entrapped at blueschist to eclogite transition: evidence from the Tianshan meta-subduction complex in northwestern China. Contributions to Mineralogy and Petrology, 142, 1-14.

Gao, J., John, T., Klemd, R., and Xiong, X. (2007) Mobilization of Ti-Nb-Ta during subduction: evidence from rutile-bearing dehydration segregations and veins hosted in eclogite, Tianshan, NW China. Geochimica et Cosmochimica Acta, 71, 4974-4996.

Gao, X.Y., Zheng, Y.F., and Chen, Y.X. (2012) Dehydration melting of ultrahigh-pressure eclogite in the Dabie orogen: evidence from multiphase solid inclusions in garnet. Journal of Metamorphic Geology, 30.

Garrido, C.J., López Sánchez-Vizcaíno, V., Gómez-Pugnaire, M.T., Trommsdorff, V., Alard, O., Bodinier, J.L., and Godard, M. (2005) Enrichment of HFSE in chlorite–harzburgite produced by high-pressure dehydration of antigorite–serpentinite: implications for subduction magmatism. Geochemistry, Geophysics, Geosystems, 6, http://dx.doi.org/10.1029/2004GC000791.

Giaramita, M.J., and Sorensen, S.S. (1994) Primary fluids in low-temperature eclogites: evidence from two subduction complexes (Dominican Republic, and California, USA). Contributions to Mineralogy and Petrology, 117, 279-292.

Gorman, P.J., Kerrick, D.M., and Connolly, J.A.D. (2006) Modeling open system metamorphic decarbonation of subducting slabs. Geochemistry Geophysics Geosystems, 7, p. Q04007.

Groppo, C., Beltrando, M., and Compagnoni, R. (2009) The P-T path of the ultra-high pressure Lago di Cignana and adjoining high-pressure meta-ophiolitic units: insights into the evolution of the subduction Tethyan slab. Journal of Metamorphic Geology, 27, 207-231.

Hack, A.C., and Thompson, A.B. (2011) Density and viscosity of hydrous magmas and related fluids and their role in subduction zone processes. Journal of Petrology, 52, 1333-1362.

Hack, A.C., Hermann, J., and Mavrogenes, J.A. (2007a) Mineral solubility and hydrous melting relations in the deep earth: analysis of some binary A-H_2O system pressure-temperature-composition topologies. American Journal of Science, 307, 833-855.

Hack, A.C., Thompson, A.B., Aerts, M. (2007b) Phase relations involving hydrous silicate melts,

aqueous fluids, and minerals, Reviews in Mineralogy and Geochemistry, 65, 129-177.

914 Hacker, B.R., Abers, G.A., and Peacock, S.M. (2003) Subduction factory 1. Theoretical
915 mineralogy, densities, seismic wave speeds and H_2O contents. Journal of Geophysical Research,
916 108, 2029-2054.

917 Haefner, A. Aranovich, L.Y., Connolly J.A.D., and Ulmer, P. (2002) H_2O activity in H_2O-N_2 fluids
918 at high pressure and temperature measured by the brucite periclase equilibrium. American
919 Mineralogist, 87, 822-828.

920 Haendel, D., Muhle, K., Nitzsche, H.M., Stiehl, G., and Wand, U. (1986) Isotopic variations of the
921 fixed nitrogen in metamorphic rocks. Geochimica et Cosmochimica Acta, 50, 749-758.

922 Hallam, M., and Eugster, H.P. (1976) Ammonium silicate stability relations. Contributions to
923 Mineralogy and Petrology, 57, 227-244.

924 Halter, W.E., Pettke, T., Heinrich, C.A., and Rothen-Rutishauser, B. (2002) Major to trace element
925 analysis of melt inclusions by laser-ablation ICPMS: methods of quantification. Chemical Geology,
926 183, 63-86.

927 Heinrich, W. (2007) Fluid immiscibility in metamorphic rocks. In A. Liebscher, and C.A. Heinrich,
928 Eds. Fluid-fluid interactions, 65, p. 389-430. Reviews in Mineralogy and Geochemistry,
929 Mineralogical Society of America.

930 Heinrich, W., and Gottschalk, M. (1995) Metamorphic reactions between fluid inclusions and
931 mineral hosts I: Progress of the reaction calcite + quartz <==> wollastonite + CO_2 in natural
932 wollastonite-hosted fluid inclusions. Contributions to Mineralogy and Petrology, 122, 51-61.

933 Hermann, J. (2002a) Experimental constraints on phase relations in subducted continental crust.
934 Contributions to Mineralogy and Petrology, 143, 219-235.

935 Hermann, J. (2002b) Allanite:thorium and light rare earth element carrier in subducted crust.
936 Chemical Geology, 192, 289-306.

937 Hermann, J. (2003) Experimental evidence for diamond-facies metamorphism in the Dora-Maira
938 massif. Lithos, 70, 163-182.

939 Hermann, J., and Rubatto, D. (2009) Accessory phase control on the trace element signature of
940 sediment melts in subduction zones. Chemical Geology, 265, 512-526.

941 Hermann, J., and Spandler, C. (2008) Sediment melts at sub-arc depths: an experimental study.
942 Journal of Petrology, 49, 717-740.

943 Hermann, J., Spandler, C., Hack, A.C., and Korsakov, A.V. (2006) Aqueous fluids and hydrous
944 melts in high-pressure and ultra-high pressure rocks: implications for element transfer in subduction
945 zones. Lithos, 92, 399-417.

946 Hermann, J., Zheng, Y.F., and Rubatto, D. (2013) Deep fluids in subducted continental crust.
947 Elements, 9, 281-287.

948 Hidas, K., Guzmics, T., Szabó, C., Kovács, I., Bodnar, R.J., Zajacz, Z., Nédli, Z., Vaccari, L., and
949 Perucchi, A. (2010) Coexisting silicate melt inclusions and H_2O-bearing, CO_2-rich fluid inclusions

in mantle peridotite xenoliths from the Carpathian–Pannonian region (central Hungary). Chemical Geology, 274, 1-18.

Hunt, J.D., and Manning, C.E. (2012) A thermodynamic model for the system SiO_2–H_2O near the upper critical end point based on quartz solubility experiments at 500–1100 °C and 5–20 kbar. Geochimica et Cosmochimica Acta, 86, 196-213.

Hwang, S., Shen, P., Chu, H., Yui, T., and Lin, C. (2001) Genesis of microdiamonds from melt and associated multiphase inclusions in garnet of ultrahigh-pressure gneiss from Erzgebirge, Germany. Earth and Planetary Science Letters, 188, 9-15.

Hwang, S., Shen, P., Yui, T., and Chu, H. (2003) Metal-sulfur-COH-silicate fluid mediated diamond nucleation in Kokchetav ultrahigh-pressure gneiss. European Journal of Mineralogy, 15, 503-511.

Hwang, S., Shen, P., Chu, H., Yui, T., Liou, J.G., Sobolev, N.V., Zhang, R.Y., Shatsky, V.S., and Zayachkovsky, A.A. (2004) Kokchetavite: a new potassium-feldspar polymorph from the Kokchetav ultrahigh-pressure terrane. Contributions to Mineralogy and Petrology, 148, 380-389.

Hwang, S., Shen, P., Chu, H., Yui, T., Liou, J.G., Sobolev, N.V., and Shatsky, V.S. (2005) Crust-derived potassic fluid in metamorphic microdiamond. Earth and Planetary Science Letters, 231, 295-306.

Hwang, S., Chu, H., Yui, T., Shen, P., Schertl, H.P., Liou, J.G., and Sobolev, S.V. (2006) Nanometer-size P/K-rich silica glass (former melt) inclusions in microdiamond from the gneisses of Kokchetav and Erzgebirge massifs: diversified characteristics of the formation media of metamorphic microdiamond in UHP rocks due to host-rock buffering. Earth and Planetary Science Letters, 243, 94-106.

Iler, R.K. (1979) The chemistry of silica: solubility, polymerization, colloid and surface properties, and biochemistry. 866 p. Wiley.

Johnson, M.C., and Plank, T. (1999) Dehydration and melting experiments constrain the fate of subducted sediments. Geochemistry Geophysics Geosystems, 1, doi: 10.1029/1999GC000014

Kawamoto, T. (2006) Hydrous phases and water transport in the subducting slab. In H. Keppler, and J.R. Smyth, Eds. Water in nominally anhydrous minerals., 62, p. 273-289. Reviews in Mineralogy and Geochemistry, Mineralogical Society of America.

Kawamoto, T., Kanzaki, M., Mibe, K., Matsukage, N.K., and Ono, S. (2012) Separation of supercritical slab-fluids to form aqueous fluid and melt components in subduction zone magmatism. Proceedings of the National Academy of Sciences, 109, 18695-18700.

Kennedy, G.C., Wasserburg, G.J., Heard, H.C., and Newton, R.C. (1962) The upper three-phase region in the system SiO2-H2O. American Journal of Science, 260, 501-521.

Kerrick, D.M., and Connolly, J.A.D. (2001), Metamorphic devolatilization of subducted oceanic metabasalts:Implications for seismicity, arc mag- matism and volatile recycling, Earth and Planetary Science Letters, 189,19–29.

Kessel, R., Schmidt, M.W., Ulmer, P., and Pettke, T. (2005a) Trace element signature of subduction-zone fluids, melts and supercritical liquids at 120-180 km depth. Nature, 437, 724-727.

Kessel, R., Ulmer, P., Pettke, T., Schmidt, M.W., and Thompson, A.B. (2005) The water-basalt system at 4 to 6 GPa: phase relations and second critical end-point in a K-free eclogite at 700 to 1400 °C. Earth and Planetary Science Letters, 237, 875-892.

Klemd, R. (1989) P-T evolution and fluid inclusion characteristics of retrograded eclogites, Münchberg Gneiss Complex, Germany. Contributions to Mineralogy and Petrology, 102, 221-229.

Klemd, R. (2013) Metasomatism During High-Pressure Metamorphism: Eclogites and Blueschist-Facies Rocks. In D.E. Harlow, and H. Austrheim, Eds. Metasomatism and the Chemical Transformation of Rock. The role of fluids in Terrestrial and extraterrestrial processes. p. 351-414. Springer-Verlag, Berlin Heidelberg.

Klemd, R., van den Kerkhof, A.M., and Horn, E.E. (1992) High-density CO_2-N_2 inclusions in eclogite-facies metasediments of the Münchberg gneiss complex, SE Germany. Contributions to Mineralogy and Petrology, 111, 409-419.

Klemd, R., Bröcker, M., and Schramm, J. (1995) Characterisation of amphibolite-facies fluids of Variscan eclogites from the Orlica-Snieznik dome (Sudetes, SW Poland). Chemical Geology, 119, 101-113.

Korsakov, A.V., and Hermann, J. (2006) Silicate and carbonate melt inclusions associated with diamond in deeply subducted carbonate rocks. Earth and Planetary Science Letters, 241, 104-118.

Kretz, R. (1983) Symbols for rock-forming minerals. American Mineralogist, 68, 277-279.

Lang, H.M., and Gilotti, J.A. (2007) Partial melting of metapelites at ultrahigh-pressure conditions, Greenland Caledonides. Journal of Metamorphic Geology, 25, 129-147.

Liebscher, A. (2010) Aqueous fluids at elevated pressure and temperature. Geofluids, 10, 3-19.

Liu, Q., Hermann, J., and Zhang, J. (2013) Polyphase inclusions in the Shuanghe UHP eclogites formed by sub-solidus transformation and incipient melting during exhumation of deeply subducted crust. Lithos, 177, 91-109.

Malaspina, N., Hermann, J., Scambelluri, M., and Compagnoni, R. (2006) Polyphase inclusions in garnet-orthopyroxenite (Dabie Shan, China) as monitors for metasomatism and fluid-related trace element transfer in subduction zone peridotite. Earth and Planetary Science Letters, 249, 173-187.

Malaspina, N., Hermann, J., and Scambelluri, M. (2009) Fluid/mineral interaction in UHP garnet peridotite. Lithos, 107, 38-52.

Malaspina, N., Scambelluri, M., Poli, S., van Roermund, H.L.M., and Langenhorst, F. (2010) The oxidation state of mantle wedge majoritic garnet websterites metasomatised by C-bearing subduction fluids. Earth and Planetary Science Letters, 298, 417-126.

Manning, C.E. (1998) Fluid composition at the blueschist-eclogite transition in the model system Na_2O-MgO-Al_2O_3-SiO_2-H_2O-HCl. Schweizerische Mineralogische und Petrographische Mitteilungen, 78, 225-242.

Manning, C.E. (2004) The chemistry of subduction-zone fluids. Earth and Planetary Science Letters, 223, 1-16.

Manning, C. E., Shock, E. L., and Sverjensky, D. A. (2013) The chemistry of carbon in aqueous fluids at crustal and upper-mantle conditions: Experimental and theoretical constraints. Reviews in Mineralogy and Geochemistry 75, 109–148.

Martin, L.A.J., Wood, B.J., Turner, S., and Rushmer, T. (2011) Experimental measurements of trace element partitioning between lawsonite, zoisite and fluid and their implication for the composition of arc magmas. Journal of Petrology, 52, 1049-1075.

McDonough, W.F., and Sun, S.S. (1995) Composition of the earth. Chemical Geology, 120, 223-253.

Mibe, K., Kawamoto, T., Matsukage, N.K., Fei, Y., and Ono, S. (2011) Slab melting versus slab dehydration in subduction-zone magmatism. Proceedings of the National Academy of Sciences, 108, 8177-8182.

Molina, J.F., and Poli, S. (2000) Carbonate stability and fluid composition in subducted oceanic crust: An experimental study on H_2O-CO_2-bearing basalts. Earth and Planetary Science Letters 176, 295-310.

Mposkos, E., Perraki, M., and Palikari, S. (2009) Single and multiphase inclusions in metapelitic garnets of the Rhodope Metamorphic Province, NE Greece. Spectrochimica Acta Part A: molecular and biomolecular spectroscopy, 73, 477-483.

Mukherjee, B.K., and Sachan, H.K. (2009) Fluids in coesite-bearing rocks of the Tso Morari Complex, NW Himalaya: evidence for entrapment during peak metamorphism and subsequent uplift. Geological Magazine, 146, 876-889.

Mysen B.O. (2010) Speciation and mixing behavior of silica-saturated aqueous fluid at high temperature and pressure. American Mineralogist, 95, 1807-1816.

Mysen, B.O. (2012) Silicate-COH melt and fluid structure, their physicochemical properties, and partitioning of nominally refractory oxides between melts and fluids. Lithos, 148, 228-246.

Mysen, B.O., and Shang, J. (2003) Fractionation of major elements between coexisting H_2O-saturated silicate melt and silicate-saturated aqueous fluids in allumosilicate systems at 1-2 GPa. Geochimica et Cosmochimica Acta, 67, 3925-3936.

Naemura, K., Hirajima, T., and Svojtka, M. (2009) The Pressure-Temperature Path and the Origin of Phlogopite in Spinel-Garnet Peridotites from the Blanský Les Massif of the Moldanubian Zone, Czech Republic. Journal of Petrology, 50, 1795-1827.

Newton, R.C., and Manning, C.E. (2002) Solubility of enstatite + forsterite in H_2O at deep crust/upper mantle conditions: 4 to 15 kbar and 700 to 900°C. Geochimica et Cosmochimica Acta, 66, 4165-4176.

Newton, R.C., and Manning, C.E. (2003) Activity coefficient and polymerization of aqueous silica at 800 °C. 12 kbar, from solubility measurements on SiO_2-buffering mineral assemblages. Contributions to Mineralogy and Petrology, 146, 135-143.

Newton, R. C., and Manning, C. E. (2008) Thermodynamics of SiO_2-H_2O fluid near the upper critical end point from quartz solubility measurements at 10 kbar. Earth and Planetary Science Letters, 274, 241-249.

Newton, R.C., and Manning, C.E. (2010) Role of saline fluids in deep-crustal and upper-mantle metasomatism: insight from experimental studies. Geofluids, 10, 57-72.

Paillat, O., Elphick, S.C., and Brown, W.L. (1992) The solubility of water in $NaAlSi_3O_8$ melts: a re-examination of Ab-H2O phase relationship and critical behaviour at high pressures. Contributions to Mineralogy and Petrology, 112, 490-500.

Pan, D., Spanu, L., Harrison, B., Sverjensky, D.A., and Galli, G. (2013) Dielectric properties of water under extreme conditions and transport of carbonates in the deep Earth. Proceedings of the National Academy of Sciences of the United States of America, 110, 6646-6650.

Philippot, P. (1993) Fluid-melt-rock interaction in mafic eclogites and coesite-bearing metasediments: constraints on volatile recycling during subduction. Chemical Geology, 108, 93-112.

Philippot, P., and Selverstone, J. (1991) Trace-element-rich brines in eclogitic veins: implications for fluid composition and transport during subduction. Contributions to Mineralogy and Petrology, 106, 417-430.

Philippot, P., Chevallier, P., Chopin, C., and Dubessy, J. (1995) Fluid composition and evolution in coesite-bearing rocks (Dora-Maira massif, Western Alps): implications for element recycling during subduction. Contributions to Mineralogy and Petrology, 121, 29-44.

Philippot, P., Agrinier, P., and Scambelluri, M. (1998) Chlorine cycling during subduction of altered oceanic crust. Earth and Planetary Science Letters, 161, 33-44.

Poli, S., and Schmidt, M.W. (2002) Petrology of subducted slabs. Annual Review of Earth and Planetary Sciences, 30, 207-235.

Poli, S., Franzolin, E., Fumagalli, P., and Crottini, A. (2009) The transport of carbon and hydrogen in subducted oceanic crust: An experimental study to 5 GPa. Earth and Planetary Science Letters, 278, 350-360.

Pöter, B., Gottschalk, M., and Heinrich, W. (2004) Experimental determination of the ammonium partitioning among muscovite, K-feldspar, and aqueous chloride solutions. Lithos, 74, 67-90.

Roedder, E. (1984) Fluid inclusions. Review in Mineralogy, 12, p. 678. Mineralogical Society of America, Washington.

Rubatto, D., and Hermann, J. (2001) Exhumation as fast as subduction? Geology, 29, 3-6.

Rubatto, D., and Hermann, J. (2003) Zircon formation during fluid circulation in eclogites (Monviso, Western Alps): implicationsfor Zr and Hf budget in subduction zones. Geochimica et Cosmochimica Acta, 67, 2173–2187.

Rudnick, R., Barth, M., Horn, I., and McDonough, W. (2000) Rutile-bearing refractory eclogites: Missing link between continents and depleted mantle: Science, 287, 278–281,

Ryabchikov, I.D. (1993) Fluid transport of ore metals in ultramafic mantle rocks. Proceedings of the Eight Quadriennial IAGOD Symposium, p. 425-433.

Sanchez-Valle, C. (2013) Structure and thermodynamics of subduction zone fluids from spectroscopic studies. In A. Stefánsson, T. Driesner, and P. Bénézeth, Eds. Thermodynamics of geothermal fluids., 76, p. 265-309. Reviews in Mineralogy and Geochemistry, Mineralogical Society of America.

Sanchez-Valle, C., Mantegazzi, D., and Driesner, T. (2013) Thermodynamics of carbon-bearing fluids and oxidised carbon speciation equilibria in subduction zone fluids. Goldschmidt 2013 Conference Abstract, p. 2125.

Scambelluri, M., and Philippot, P. (2001) Deep fluids in subduction zones. Lithos, 55, 213-227.

Scambelluri, M., Piccardo, G.B., Philippot, P., Robbiano, A., and Negretti, L. (1997) High salinity fluid inclusions formed from recycled seawater in deeply subducted alpine serpentinite. Earth and Planetary Science Letters, 148, 485-499.

Scambelluri, M., Pennacchioni, G., and Philippot, P. (1998) Salt-rich aqueous fluids formed during eclogitization of metabasites in the Alpine continental crust (Austroalpine Mt. Emilius unit, Italian western Alps). Lithos, 43, 151-167.

Scambelluri, M., Bottazzi, P., Trommsdorff, V., Vannucci, R., Hermann, J., Gomez-Pugnaire, M.T., and Lòpez-Sànchez Vizcaìno, V. (2001) Incompatible element-rich fluids released by antigorite breakdown in deeply subducted mantle. Earth and Planetary Science Letters, 192, 457-470.

Schmidt, M.W., and Poli, S. (1998) Experimentally based water budgets for dehydrating slabs and consequences for the arc magma generation. Earth and Planetary Science Letters, 163, 361-379.

Schmidt, M.W., and Poli, S. (2003) Generation of mobile components during subduction of oceanic crust. In R.L. Rudnick, Ed. The Crust, 3, p. 567-591. Elsevier-Pergamon, Oxford.

Schmidt, M.W., Vielzeuf, D., and Auzanneau, E. (2004) Melting and dissolution of subducting crust at high pressures: the key role of white mica. Earth and Planetary Science Letters, 65-84.

Selverstone, J., Franz, G., Thomas, S., and Getty, S. (1992) Fluid variability in 2 GPa eclogites as indicator of fluid behaviour during subduction. Contributions to Mineralogy and Petrology, 112, 341-357.

Sharp, Z.D., and Barnes, J.D. (2004) Water-soluble chlorides in massive seafloor serpentinites: a source of chloride in subduction zones. Earth and Planetary Science Letters, 226, 243-254.

Shen, K., Zhang, Z.M., van den Kerkhof, A.M., Xiao, Y., Xu, Z.Q., and Hoefs, J. (2003) Unusual high-density and saline aqueous inclusions in ultra-high pressure metamorphic rocks from Su-Lu terrane, in eastern China. Chinese Science Bulletin, 48, 2018-2023.

Sorby, H.C. (1858) On the microscopic structures of crystals, indicating the origin of minerals and rocks. Quarterly Journal of the Geological Society of London, 14, 453-500.

Spandler, C., and Pirard, C. (2013) Element recycling from subducting slabs to arc crust: a review. Lithos, 170-171, 208-223.

Spandler, C., Mavrogenes, J.A., and Hermann, J. (2007) Experimental constraints on element mobility from subducted sediments using high-P synthetic fluid/melt inclusions. Chemical Geology, 239, 228-249.

Stalder, R., Ulmer, P., Thompson, A.B., and Gunther, G. (2000) Experimental approach to constrain second critical end points in fluid/silicate systems: near-*solidus* fluids and melts in the system albite-H_2O. American Mineralogist, 85, 68-77.

Stalder, R., Ulmer, P., Thompson, A.B., and Gunther, G. (2001) High pressure fluids in the system MgO-SiO_2-H_2O under upper mantle conditions. Contributions to Mineralogy and Petrology, 140, 607-618.

Sterner, S.M., and Bodnar, R.J. (1991) Synthetic fluid inclusions – VII. Re-equilibration of fluid inclusions in quartz during laboratory simulated burial and uplift. Journal of Metamorphic Geology, 7, 243-260.

Stöckhert, B., Duyster, J., Trepmann, C., and Massonne, H.J. (2001) Microdiamond daughter crystals precipitated from supercritical COH + silicate fluids included in garnet, Erzgebirge, Germany. Geology, 29, 391-394.

Stöckhert, B., Trepmann, C.A., and Massonne, H.J. (2009) Decrepitated UHP fluid inclusions: about diverse phase assemblages and extreme decompression rates (Erzgebirge, Germany). Journal of Metamorphic Geology, 27, 673-684.

Svensen, H., Jamtveit, B., Yardley, B.W.D., Engvik, A.K., Austrheim, H., and Broman, C. (1999) Lead and bromine enrichement in eclogite-facies fluids: extreme fractionation during lower-crustal hydration. Geology, 27, 467-470.

Svensen, H., Jamtveit, B., Banks, D.A., and Austrheim, H. (2001) Halogen contents of eclogite facies fuid inclusions and minerals: Caledonides, western Norway. Journal of Metamorphic Geology, 19, 165-178.

Touret, J.L.R. (2001) Fluids in metamorphic rocks. Lithos, 55, 1-25.

Touret, J.L.R., and Frezzotti, M.L. (2003) Fluid inclusions in high pressure and ultrahigh pressure metamorphic rocks. In D.A. Carswell, and R. Compagnoni, Eds. Ultrahigh-pressure metamorphism. E.M.U. Notes in Mineralogy, 5, p. 467-487.

Ulmer, P. (2001) Partial melting in the mantle wedge – the role of H2O in the genesis of mantle-derived 'arc-related' magmas. Physics of the Earth and Planetary Interiors, 127, 215-232.

Vallis, F., and Scambelluri, M. (1996) Redistribution of high-pressure fluids during retrograde metamorphism of eclogite-facies rocks (Voltri Massif, Italian Western Alps). Lithos, 39, 81-92.

van den Kerkhof, A.M., and Hein, U.F. (2001) Fluid inclusion petrography. Lithos, 55, 27-47.

van Roermund, H.L.M., Carswell, D.A., Drury, M.R., and Heijboer, T.C. (2002) Microdiamond in a megacrystic garnet websterite pod from Bardane on the island of Fjørtoft, western Norway: evidence for diamond formation in mantle rocks during deep continental subduction. Geology, 30, 959-962.

Viti, C., and Frezzotti M.L. (2000) Re-equilibration of glass and CO_2 inclusions in xenolith olivine: A TEM study, American Mineralogist, 85, 1390–1396.

Viti, C., and Frezzotti, M.L. (2001) Transmission electron microscopy applied to fluid inclusion investigations. Lithos, 55, 125-138.

Vrijmoed, J.C., Smith, D.C., and Van Roermund, H.L.M. (2008) Raman confirmation of microdiamond in the Svartberget Fe-Ti type garnet peridotite, Western Gneiss Region, Western Norway. Terra Nova, 20, 295-301

Whitney, D.L., and Evans, B.W. (2010) Abbreviations for names of rock-forming minerals. American Mineralogist, 95, 185-187.

Wilke, M., Schmidt, C., Dubrail, J., Appel, K., Borchert, M., Kvashnina, K., and Manning, C.E. (2012) Zircon solubility and zirconium complexation in $H_2O + Na_2O + SiO_2 \pm Al_2O_3$ fluids at high pressure and temperature. Earth and Planetary Science Letters, 349-350, 15-25.

Xiao, Y.L., Hoefs, J., van den Kerkhof, A.M., Fiebig, J., and Zheng, Y.F. (2000) Fluid history of UHP metamorphism in Dabie Shan, China: a fluid inclusion and oxygen isotope study on the coesite-bearing eclogite from Bixiling. Contributions to Mineralogy and Petrology, 139, 1-16.

Xiao, Y.L., Hoefs, J., Van den Kerkhof, A.M., and Li, S.G. (2001) Geochemical constraints of the eclogite and granulite facies metamorphism as recognized in the Raobazhai complex from North Dabie Shan, China. Journal of Metamorphic Geology, 19, 3-19.

Xiao, Y.L., Hoefs, J., Van den Kerkhof, A.M., Simon, K., Fiebig, J., and Zheng, Y.F. (2002) Fluid evolution during HP and UHP metamorphism in Dabie Shan, China: constraints from mineral chemistry, fluid inclusions and stable isotopes. Journal of Petrology, 43, 1505-1527.

Xiao, Y.L., Zhang, Z.M., Hoefs, J., and Van den Kerkhof, A.M. (2006) Ultrahigh-pressure metamorphic rocks from the Chinese Continental Scientific Drilling Project: II oxygen isotope and

fluid inclusion distributions through vertical sections. Contributions to Mineralogy and Petrology, 152, 443-458.

Xu, L., Sun, X.M., Zhai, W., Liang, J.L., Liang, Y.H., Shen, K., Zhang, Z.M., and Tang, Q. (2006) Fluid inclusions in quartz veins from HP-UHP metamorphic rocks, Chinese Continental Scientific Drilling (CCSD) project. International Geology Review, 48, 639-649.

Yang, X.Y., Zheng, Y.F., Liu, D., and Dai, J. (2001) Chemical and carbon isotope compositions of fluid inclusions in peridotite xenoliths and eclogites from eastern China: Geodynamic implications. Physic and Chemistry of Earth (A), 26, 705-718.

Yardley, B.W.D. (2013). The chemical composition of metasomatic fluids in the crust. In D.E. Harlow, and H. Austrheim, Eds. Metasomatism and the Chemical Transformation of Rock. The role of fluids in Terrestrial and extraterrestrial processes. p. 17–51. Springer-Verlag, Berlin Heidelberg.

Zeng, L.S., Liang, F.H., Asimov, P.D., Chen, F.Y., and Chen, J. (2009) Partial melting of deeply subducted continental crust and the formation of quartzofeldspathic polyphase inclusions in the Sulu UHP eclogites. Chinese Science Bulletin, 54, 2580-2594.

Zhang, Z.M., Shen, K., Xiao, Y., Van den Kerkhof, A.M., Hoefs, J., and Liou, J.G. (2005) Fluid composition and evolution attending UHP metamorphism: study of fluid inclusions from Drill Cores, Southern Sulu Belt, Eastern China. International Geology Review, 47, 297-309.

Zhang, Z.M., Shen, K., Sun, W.D., Liu, Y.S., Liou, J.G., Shi, C., and Wang, J.L. (2008) Fluid in deeply subducted continental crust: petrology, mineral chemistry and fluid inclusion of UHP metamorphic veins from the Sulu orogen, eastern China. Geochimica et Cosmochimica Acta, 72, 3200-3228.

Zhang, Z.M., Shen, K., Liou, J.G., Dong, X., Wang, W., Yu, F., and Liu, F. (2011) Fluid–rock interactions during UHP metamorphism: a review of the Dabie–Sulu orogen, east-central China. Journal of Asian Earth Sciences, 42, 316-129.

Zheng, Y.F., Xia, Q.X., Chen, R.X., and Gao, X.Y. (2011) Partial melting, fluid supercriticality and element mobility in ultrahigh-pressure metamorphic rocks during continental collision. Earth-Science Reviews, 107, 342-374.

Zotov, N., and Keppler, H. (2002) Silica speciation in aqueous fluids at high pressures and high temperatures. Chemical Geology, 184, 71-82.

CAPTIONS TO FIGURES

Figure 1: Photomicrographs of primary fluid inclusions (FI) in eclogite-facies H*P*-UH*P* rocks. (a) Aqueo-carbonic FI elongated parallel to the c-axis of the host OH-rich topaz. Liquid and gaseous CO_2 corresponds to about 30 % of the inclusion total volume. The two

1230 solids are a chloride (s) and gypsum. OH-rich topaz – kyanite quartzite from Sulu, China
1231 (sample RPC546, Plane Polarised Light, PPL). Modified from Frezzotti et al. (2007). (b)
1232 Diamond-bearing aqueous FI in garnet [liquid (L) + vapor (V) > 60% of the total volume of
1233 the inclusions]. Garnetite nodules from Lago di Cignana, Italian western Alps (sample C2BA,
1234 PPL). (c) Chloride-bearing aqueous FI in epidote. L + V represent about 80% of the inclusion
1235 total volume. Two isotropic salts (s) are also present. Phengite-kyanite-epidote eclogite from
1236 Sulu, China (sample RPC778, PPL). Modified from Ferrando et al. (2005a). (d) Chloride-
1237 bearing aqueous FIs elongated parallel to the c-axis of the host kyanite. L+V represent about
1238 40% of the inclusion total volume. Paragonite and ellenbergerite are the solid phases. Pyrope
1239 whiteschists from Dora-Maira, Italian western Alps (sample DM1598, PPL). Modified from
1240 Ferrando et al. (2009).

1241 Figure 2: Photomicrographs of preserved primary multiphase solid inclusions (MSI).
1242 (a) MSI in kyanite showing negative crystal shape. It contains the typical association of
1243 paragonite + muscovite + anhydrite + “alunite”-type sulfate + pyrite + small volume of an
1244 aqueous fluid. OH-rich topaz – kyanite quartzite from Sulu, China (sample RPC547, PPL). (b)
1245 MSI in garnet showing negative crystal shape. They are filled by paragonite + phlogopite +
1246 diamond + quartz + apatite + rutile without apparent fluid. Garnet gneiss, Saxonian
1247 Erzgebirge (sample RAR10, PPL). (c) Back-scattered electron (BSE) image of a freshly-
1248 broken surface of a pyrope including a MSI. Note the preferred orientation of Mg-chlorite and
1249 Na-K-phlogopite. Pyrope whiteschists from Dora-Maira, Italian western Alps (sample
1250 DM69). Modified from Ferrando et al. (2009). (d) MSI in garnet showing negative crystal
1251 shape. In this case, the oriented intergrowth described in Fig. 2c is recognizable also under the
1252 microscope. Pyrope whiteschists from Dora-Maira, Italian western Alps (sample DM1035)

1253 Figure 3: Photomicrographs (PPL: a, d; crossed polarizer: b, e) and back-scattered
1254 images (c, f) of two preserved primary MSI in pyrope from a Dora-Maira whiteschist. Both

MSI have negative crystal shapes and are filled by of Mg-chlorite, Na-K-phlogopite, apatite and pyrite showing periodic crystallization, without any visible fluid phase. Pyrope whiteschists from Dora-Maira, Italian western Alps (a, b, and c: MSI in sample DM1035; d, e, and f: MSI in sample DM1042). Modified from Frezzotti and Ferrando (2007).

Figure 4: Photomicrographs (PPL) of a primary melt inclusion in quartz from Mt. Genis granite (Sardinia, Italy). (a) At magmatic conditions (900°C), the inclusion consists of immiscible silicate-melt and hypersaline fluid. (b) At 20°C, the melt phase is crystallized in a fine-grained aggregate of randomly oriented anhedral to subhedral crystals, coexisting with chlorides, and liquid H_2O. Modified from Frezzotti (2001).

Figure 5: Photomicrographs showing petrographic features of MSI. (a) Primary MSI in kyanite. Inclusions have the same dimensions and are oriented along the c axis of the host mineral. OH-rich topaz – kyanite quartzite from Sulu, China (sample RPC 547, PPL). Modified from Frezzotti and Ferrando (2007). (b) Distribution of primary MSI marking the growth zones of the host garnet. Pyrope whiteschists from Dora-Maira, Italian western Alps (sample DM1616, PPL). (c) BSE image of a MSI in pyrope, containing a large incidentally-trapped rutile. Pyrope whiteschists from Dora-Maira, Italian western Alps (sample DM69). Modified from Ferrando et al. (2009).

Figure 6: Collages of BSE images of MSI on an EMP Ca-distribution map of the host garnet (courtesy of B. Stöckhert), showing abundance and the primary distribution of the MSI. The MSI are filled by silicates (quartz + white micas, locally retrogressed) + apatite + rutile ± diamond/graphite. Some inclusions still preserve a negative crystal shape. Other inclusions show reentrant angles at grain edges between inclusion minerals and host garnet and development of offshoots from the corners. Other inclusions show a star-shaped contour with short and thin microfractures lining from the corners. The distribution of the inclusion

types is not systematic. Quartzofeldspathic rock, Saxonian Erzgebirge (modified from Stöckhert et al. 2009).

Figure 7: Outline of the most important post-trapping modifications that can occur in a MSI during exhumation. Stage 1: Fluid trapping. Stage 2: Periodic crystallization of daughter minerals and dissolution and precipitation of the host mineral on the inclusion walls. Stage 3: Early decrepitation event, occurring at the UH*P*-H*P* transition, that can induce i) formation of short and large fractures (offshoots) departing from the inclusion corners, ii) crystallization of step-daughter minerals and partial re-crystallization of the host mineral producing irregular contours and re-entrant angles in the MSI, and/or iii) diffusion of water into the host mineral (see, Fig. 10). Stage 4: Daughter mineral crystallization leaves a residual fluid that may produce retrograde metamorphic reactions inside MSI. Stage 5: Late decrepitation event at L*P*, characterized by the formation of microfractures containing trails of small fluid inclusions, haloes of small fluid inclusions distributed around the inclusion, and/or star-shaped contours in MSI. The BSE image shows a MSI that experienced most of the described post-trapping modifications (see, Fig. 8a, and its caption).

Figure 8: Photomicrographs showing post-trapping modifications in MSI. (a) BSE image of a decrepitated MSI in kyanite, showing minerals and cavities (black). The inclusion is characterized by the typical oriented association of daughter-minerals. Post-crystallization hydration reactions occurred on corundum to form diaspore. Decrepitation features (offshoots and microfractures) are also recognizable. OH-rich topaz – kyanite quartzite from Sulu, China (sample RPC 547). Modified from Ferrando et al. (2005b). (b) Fan-shaped chemical re-equilibration of the host garnet around a MSI. Pyrope whiteschists from Dora-Maira, Italian western Alps (sample DM14, PPL). PPL (c) and BSE (d) images of a MSI in garnet that experienced different post-trapping modifications. A non-equilibrium growth of the host mineral on the inclusion wall produced irregular and re-entrant contours. Subsequent

decrepitation produced microfractures lining from the corners and loss of fluid (FI) and Ca-enrichment in the host garnet. Ky-Phe-Ep eclogite from Sulu, China (sample RPC 778). Modified from Ferrando et al. (2005b). (e) MSI with irregular contours due to a non-equilibrium growth of the host mineral on the inclusion wall. Offshoots due to partial decrepitation are also present (thick arrows). OH-rich topaz – kyanite quartzite from Sulu, China (sample RPC547, PPL). (f) Aqueo-carbonic fluid inclusion in quartz. Irregular contours and reentrant angles are produced by the non-equilibrium growth of the host mineral on the inclusion wall. Alpine quartz vein (sample AV3, PPL).

Figure 9: Photomicrographs showing post-trapping modifications in FI and MSI. (a) Haloes of very small fluid inclusions distributed around single decrepitated MSI within pyrope. Note the irregular habit and the presence of some offshoots from the corners (thick arrows). Pyrope whiteschists from Dora-Maira, Italian western Alps (sample DM1598. PPL). Modified from Frezzotti and Ferrando (2007); (b) Typical example of post-trapping modifications in fluid inclusions from mantle clinopyroxene. The presence of offshoots (thick arrows) and of haloes of very small fluid inclusions is evident. Mantle xenolith from Mt. Iblei (Italy, PPL). (c) Post-entrapment re-equilibrations of a MSI in garnet. The large fracture forms a sort of offshoot and a halo of tiny fluid inclusions is also present. UHP eclogite from Western Gneiss Region (sample V2297, PPL). (d) Primary decrepitated MSI in pyrope showing irregular, star-shaped, contours. Both offshoots (thick arrows) and thin microfractures (thin arrows) are present. Pyrope whiteschists from Dora-Maira, Italian western Alps (sample DM69, PPL). (e) Decrepitated diamond-rich MSI in garnet. Thin microfractures (thin arrows) line from the star-shaped habit. Garnet gneiss, Saxonian Erzgebirge (sample RAR11, PPL). (f) Post-entrapment modification in silicate-melt inclusions in a quartz phenocrysts. The inclusions have thin microfractures (colorless arrows) lining from the inclusion apexes. Swarms of tiny fluid inclusions mantle the microfractures

and form grayish halos around the inclusion cavity. Microtonalite porphyry (Calabona, Sardinia, PPL). Modified from Frezzotti (2001).

Figure 10: Synchrotron FT-IR maps revealing the distribution and the concentrations of water in a Dora-Maira pyrope including some primary MSI (sample DM14). (a) Mapped garnet area (PPL). (b) Qualitative distribution map of liquid H_2O within MSI inclusions, revealed by absorption bands in the 3000–3500 cm^{-1} region. (c) Qualitative distribution map of OH^- (bands in the 3500–3800 cm^{-1} region), showing the hydrogen diffusion from the inclusions into the garnet. (d) Absorbance FT-IR map in the 3000–3800 cm^{-1} region and relative calculated water contents in garnet (ppm). (e) FT-IR spectrum showing the absorption bands for molecular H_2O, and for OH^-.

Figure 11: *P–T* diagram showing metamorphic evolution of UH*P* units discussed in the text. *P-T* path for the Lago di Cignana Unit is simplified from Groppo et al. (2009). *P-T* path for the Dora-Maria (Brossasco-Isasca Unit) is inferred combining data from different lithologies (whiteschist, marble, eclogite, calc-silicate rocks: Rubatto and Hermann 2001; Hermann 2003; Castelli et al. 2007; Ferrando et al. 2009). *P-T* path for quartzite and eclogite from South Sulu is simplified from Ferrando et al. (2005a) and Frezzotti et al. (2007). *P-T* path for the high-*T* (dashed line) UH*P* zones of Dabie-Sulu is simplified from Zheng et al. (2011). The colored squares on the *P-T* paths represent the trapping conditions of the fluid inclusions reported in Table 1. The compilation of melting reactions in mafic rocks (thick gray lines) and pelites (dashed gray lines) is revised after Schmidt and Poli (2003) and Zheng et al. (2011). The gray-shaded zones representing the *solidi* for H_2O-saturated crustal rocks and the phengite dehydration melting are from Bebout (2007; 2013). Mineral abbreviation after Whitney and Evans (2010) and Kretz (1983).

Figure 12: *P–T* diagram, modified from Hack and Thompson (2011), showing the silica solubility isopleths (in wt. % SiO_2) in the H_2O-SiO_2 system, the prograde subduction-

zone gradients of 5°C/km (cold subduction) and 10°C/km (typical subduction), and the P-T paths of metamorphic rocks in Fig. 11. C is the upper critical endpoint for the H_2O-SiO_2 system.

Fig. 13: Raman spectra from aqueous fluid inclusions associated with diamonds from Lago di Cignana metasediments. Modified from Frezzotti et al. (2011). a) Silica in solution within a fluid inclusion. The 773 cm^{-1} peak corresponds to the Si–O symmetric stretch of the $Si(OH)_4$ monomer, and the peak at 1,017 cm^{-1} to the deprotonated monomers ($SiO(OH)_3^-$, $SiO_2(OH)_2^{2-}$, and so on). The aqueous fluid also contains SO_4^{2-}, with Mg-calcite (MgCc) and quartz (Qtz). b) HCO_3^-, and CO_3^{2-} in solution within a fluid inclusion, containing Qtz. Asterisks indicate host-garnet Raman bands.

Fig. 14: Plot of viscosity data in the $NaAlSi_3O_8 + H_2O$ system: measured values are compared with those obtained from models for fluid and melt (modified from Hack and Thompson 2011).

Fig. 15: *In-situ* LA-ICP-MS analyses on multiphase solid inclusions. Normalizing values to the primordial mantle after McDonough and Sun (1995). (a) Trace-element concentrations in inclusions + host garnet compared with those in host garnet from mantle wedge garnet peridotites from Sulu (modified from Malaspina et al 2009; courtesy of N. Malaspina). (b) Trace-element concentrations in inclusions + host peak pyrope compared with those in host peak pyrope from continental UH*P* whiteschists from Dora-Maira. The trace-element patterns of the hosting metagranite, and of peak phengite, and prograde ellenbergerite and dumortierite are also reported. Modified from Ferrando et al. (2009).

Table 1. Collection of published data on deep fluid inclusions

OCCURRECES						SOLID PHASES										FLUID PHASES			NATURE OF FLUID PHASE
Metamorphic Belt	**Lithology**	**Peak *P-T* conditions**	**Stage of trapping** [a]	**Host mineral** [b]	**Name of the inclusions**	**silicates (hydrous)**	**silicates**	**carbonates**	**sulphates**	**sulphides**	**phosphates**	**oxides**	**chlorides**	**C phases**	**glass**	**water**	**gas**	**empty cavities**	
Oceanic crust																			
Piemonte Zone (Monviso)	eclogitic vein [1]	2.6 GPa 550°C [2]	near peak	H*P* Omp	fluid inclusions		albite sphene	calcite dolomite	anhydrite gypsum barite	pyrite	monazite	baddeleyite rutile Fe-oxydes	halite sylvite			yes			complex aqueous brines with Na, K, Ca, Mg, Fe, Si, Al, Zr, Ti, P, Ba, Ce, La, S, CO_3^{2-}
Piemonte Zone (Lago di Cignana)	Mn-nodules [3]	≥ 3.2 GPa 600°C [4]	peak	UH*P* Grt	multiphase solid inclusions	paragonite	quartz	calcite Mg-calcite rhodochrosite dawsonite dypingite	anhydrite pentahydrite			rutile		diamond carbonaceous material		with SO_4^{2-}, HCO_3^-, CO_3^{2-}, silica monomers			aqueous fluid enriched in Ca-Mg-Mn-Fe carbonate components ± Si ± Al ± Ti ± Na ± K ± S
Tauern Window	eclogitic segregation [5]	2.0 GPa 625°C [5]	peak	H*P* Omp, Ep, Ap and Dol	fluid inclusions	white mica zoisite glaucophane	kyanite omphacite	carbonates	Ca-sulphates		apatite	Fe-Ti oxydes rutile	chlorides salt-hydrated species			yes			brines with CO_2 ± N_2
Tso Morari	eclogite [6]	ca. 3.9 GPa ca. 750°C [6]	prograde	Qtz	high-salinity brines								halite			yes			high-salinity brines
	eclogite [6]	ca. 3.9 GPa ca. 750°C [6]	peak	Qtz, UH*P* Omp	gas-rich inclusions												N_2 CH_4		H_2-CH_4 fluids
Dabie-Sulu	eclogite [7]	1.9 GPa 600-730°C [7]	peak	H*P* Ep	aqueous inclusions											yes			highly saline brine-dominated fluids
Continental crust																			
Western Gneiss Region	eclogite [8, 9]	1.5-1.7 GPa 600°C [8, 9]	peak	H*P* Omp and Grt	multiphase brine fluid inclusions	amphibole epidote	K-feldspar quartz albite	calcite	gypsum	sphalerite pentlandite chalcopyrite galena		rutile ilmenite	halite Pb-Br-chlorides			brine			Na-K-Ca-brines with Br, Pb, I, F, Li, SO_4
Dora-Maira	Prp-quartzite [10, 11]	4.0-4.3 GPa 730°C [12]	prograde	H*P*-UH*P* Grt	fluid-free inclusions	talc Mg-chlorite		magnesite		opaque minerals	Mg-phosphate	opaque minerals	chloride			locally yes	CO_2		aqueo-carbonic brines with P, Mg, Na, K
	Prp-quartzite [10, 11]	4.0-4.3 GPa 730°C [12]	retrograde	palizade Qtz	salt-bearing inclusions					pyrite			halite sylvite			yes			immiscibility between saline and carbonic fluids
	Prp-quartzite [10, 11]	4.0-4.3 GPa 730°C [12]	retrograde	palizade Qtz	CO_2-rich inclusions											locally yes	CO_2		immiscibility between saline and carbonic fluids
	Prp-whiteschist [13]	4.0-4.3 GPa 730°C [12]	prograde	H*P*-UH*P* Ky	fluid inclusions	paragonite ellenbergerite							salts			yes			NaCl-$MgCl_2$-rich brines with Si and Al
	Prp-whiteschist [13]	4.0-4.3 GPa 730°C [12]	peak	UH*P* Grt	multiphase-solid inclusions	Mg-chlorite Na-K-phlogopite talc		magnesite		Zn-pyrite	Cl-apatite		very rare			yes			intermediate Al-Si aqueous solutions with Mg, Fe, Na, K, Ca, P, Cl, S, CO_3^{2-}, LILE, U, Th
Rhodope	Grt-Ky-Bt gneiss [14]	ca 4.5 GPa ca 1000°C [14]	prograde	UH*P* Grt	multiphase inclusions	muscovite	quartz	Mg-siderite calcite rhodochrosite						graphite			CO_2		high density hydrous-carbonaceous melt rich in C, Fe, Mg, Si, Al, K
	Grt-Ky-Bt gneiss [14]	ca 4.5 GPa ca 1000°C [14]	retrograde	UH*P* Grt	multiphase inclusions	biotite muscovite	quartz kyanite zircon				apatite	rutile							melt

[a] all the inclusions considered in this work were trapped at UHP conditions or at the HP-UHP or UHP-HP transition
[b] mineral abbreviations after Kkretx (1983) and Whitney & Evans (2010)
[1] Philippot & Selverstone (1991), [2] Angiboust et al. (2012), [3] Frezzotti et al. (2011), [4] Groppo et al. (2009),
[5] Selverstone et al. (1992), [6] Mukherjee & Sachan (2009), [7] Fu et al. (2002),
[8] Svensen et al. (1999), [9] Svensen et al. (2001), [10] Philippot (1993), [11] Philippot et al. (1995),
[12] Castelli *et al.* (2007), [13] Ferrando et al (2009), [14] Mposkos et al. (2009),

Table 1. continue

Metamorphic Belt	Lithology	Peak *P-T* conditions	Trapping conditions [a]	Host mineral [b]	Name of the inclusions	silicates (hydrous)	silicates	carbonates	sulfates	sulfides	phosphates	oxides	chlorides	C phases	glass	water	gas	empty cavities	
Continental crust																			
Erzgebirge	quartz-feldspathic rocks [15]	7-8 GPa 1100°C [16]	peak	UH*P* Grt	multiphase inclusions	phlogopite paragonite	quartz zircon			ZnS	apatite	rutile		diamond					silicate melt
	Grt-gneiss [17, 18]	7-8 GPa 1100°C [16]	peak	UH*P* Grt	polyphase inclusions	phlogopite paragonite phengite	quartz				apatite	rutile		diamond graphite					supercritical COH fluid rich in K, Na, SiO_2
	quartzo-feldspatic rocks [19]	7-8 GPa 1100°C [16]	peak	Dia	nanometric inclusions		SiO_2 K-feldspar kyanite				archerite			diamond as host mineral				yes	COH-rich multicomponent fluid rich in Si, Al, K, P, Ti
	Grt-bearing gneiss [20]	7-8 GPa 1100°C [16]	peak	Dia	nanometric inclusions									diamond as host mineral	P/K-rich silica glass				P/K-rich silica melt
	Grt-Phg-Qtz feldspathic gneiss [16]	7-8 GPa 1100°C [16]	peak	Zrn	nanometric inclusions		quartz K-feldspar	$CaCO_3$ $BaCO_3$				TiO_2 Fe_xO_y	KCl	diamond	quenched matter	yes			silicic-hydrous-saline high-density fluid, i.e. a C-O-H fluid mixed with a hydrous-silicic fluid rich in Al, K and a hydrous-saline fluid rich in Cl, K, Na
	felsic gneiss [21]	4.3 - 6.0 GPa ca. 1000°C [22]	peak	UH*P* Grt, Zrn	multiple-inclusion pockets	phengite phlogopite chlorite biotite	quartz K-feldspar albite titanite				apatite	rutile		diamond					COH-rich multicomponent supercritical fluid
	felsic gneiss [21]	4.3 - 6.0 GPa ca. 1000°C [22]	peak	Dia	nanometric inclusions	phengite phlogopite chlorite biotite	SiO_2 Fe-rich pyroxene zircon	$MgCO_3$	$BaSO_2$		apatite	Ti-oxide Cr-oxide Fe oxide Th-oxide		diamond as host mineral				yes	COH-rich multicomponent supercritical fluid
	Grt-Cpx-Qtz rocks [23]	4.3 - 6.0 GPa ca. 1000°C [22]	peak	UH*P* Grt	multiphase inclusions	phlogopite chlorite paragonite		calcite		metal sulfides				diamond					
	Grt-clinopyroxenite [24]	4.3 - 6.0 GPa ca. 1000°C [22]	peak	Dia	fluid inclusions			carbonates						diamond as host mineral		yes			C-O-H hydrous/carbonatite-like fluid
Kokchetav	Grt-Cpx rocks [25]	4.3 - 6.0 GPa ca. 1000°C [22]	retrograde	UH*P* Grt and Cpx	multiphase inclusions	phlogopite phengite talc	kokchetavite K-feldspar quartz cristobalite titanite zircon	calcite							siliceous glass				K-rich melt
	Grt-Qtz-Px rocks [20, 26]	4.3 - 6.0 GPa ca. 1000°C [22]	peak	Dia	nanometre-size inclusions									diamond as host mineral	K-rich, Si-poor glass?	K-rich, Si-poor aqueous solution?			K-rich, Si-poor fluid or melt
	Dol-marble [20, 26]	4.3 - 6.0 GPa ca. 1000°C [22]	peak	Dia	nanometre-size inclusions		silicates	carbonate	sulphates	sulphides	apatite phosphates	oxides	chlorides	diamond as host mineral		brine		yes	SiO_2-poor, ultrapotassic COH fluid with P, Cl, S
	Grt-bearing gneiss [20]	4.3 - 6.0 GPa ca. 1000°C [22]	peak	Dia	nanometric inclusions									diamond as host mineral	P/K-rich silica glass	brine			P/K-rich silica melt
	Mg-Cc marble [22]	4.3 - 6.0 GPa ca. 1000°C [22]	peak	UH*P* Grt and K-Cpx	polycrystalline & monocrystalline inclusions			Mg-calcite						diamond					carbonate melt
	Mg-Cc marble [22]	4.3 - 6.0 GPa ca. 1000°C [22]	peak	UH*P* Grt, Cpx and Ttn	polyphase inclusions	biotite	K-feldspar Cpx garnet titanite												K-rich silicate melt
	Mg-Cc marble [22]	4.3 - 6.0 GPa ca. 1000°C [22]	peak	UH*P* Grt, Cpx and Ttn	polyphase inclusions	biotite zoisite	K-feldspar titanite	Mg-calcite											K-rich silicate melt
	Dol marble [22]	4.3 - 6.0 GPa ca. 1000°C [22]	peak	UH*P* Grt	polyphase inclusions	Ti-phengite		Mg-calcite			allanite								carbonate melt

[a] all the inclusions considered in this work were trapped at UHP conditions or at the HP-UHP or UHP-HP transition
[b] mineral abbreviations after Kkretx (1983) and Whitney & Evans (2010)
[15] Hwang et al. (2001),[16] Dobrzhinetskaya et al. (2012),[17] Stöckhert et al. (2001),[18] Stöckhert et al. (2009),
[19] Dobrzhinetskaya et al. (2003b), [20] Hwang et al. (2006),[21] Dobrzhinetskaya et al. (2003a),[22] Korsakov and Hermann (2006)
[23] Hwang et al. (2003),[24] De Corte et al. (1998),[25] Hwang et al. (2004), [26] Hwang et al. (2005)

Table 1. continue

Metamorphic Belt	Lithology	Peak *P-T* conditions	Trapping conditions [a]	Host mineral [b]	Name of the inclusions	silicates (hydrous)	silicates	carbonates	sulphates	sulphides	phosphates	oxides	chlorides	C phases	glass	water	gas	empty cavities	
									Continental crust										
	eclogite [27]	2.8 - 3.3 GPa 750-800°C [27]	retrograde	UH*P* Grt	multiphase solid inclusions	epidote	k-feldspar quartz plagioclase		barite										immiscibility between aqueous fluid and hydrous silicate melt
	eclogite [28]	3.5 - 4.0 GPa 650-700°C [28]	retrograde	UH*P* Grt	polyphase inclusions	amphibole muscovite phengite	k-feldspar quartz plagioclase											yes	subsolidus breakdown products of phengite
	eclogite [28]	3.5 - 4.0 GPa 650-700°C [28]	retrograde	UH*P* Grt	polyphase inclusions		k-feldspar quartz											yes	hydrous felsic melt produced during incongruent phengite melting
	Coe-bearing eclogite [29]	3.5 - 4.0 GPa 650-700°C [28]	peak	UH*P* Omp and Ky	high-salinity aqueous inclusions								halite			yes			NaCl-dominated solutions
	Coe-eclogite [30]	3.5 - 4.0 GPa 650-700°C [28]	prograde-peak	Qtz in UH*P* Omp, UH*P* Ep and Grt	gaseous inclusions												N_2		N_2-fluids
	Coe-eclogite [30]	3.5 - 4.0 GPa 650-700°C [28]	prograde-peak	Qtz in UH*P* Omp, UH*P* Ep and Grt	high-salinity aqueous inclusions								halite			yes			high-salinity aqueous fluids
	Coe-eclogite [31]	3.5 - 4.0 GPa 650-700°C [28]	peak	Qtz, UH*P* Omp and Ky	high-salinity NaCl-dominated aqueous inclusions											yes			NaCl-dominated fluids
Dabie-Sulu	H*P* and UH*P* eclogite and Grt-clinopyroxenite [32]	≥ 2.7 GPa 630-890°C [32]	prograde-peak	UH*P* Grt, Qtz in UH*P* Grt	N_2-rich inclusions												$H_2 \pm CO_2$		N_2-rich fluids
	H*P* and UH*P* eclogite and Grt-clinopyroxenite [32]	≥ 2.7 GPa 630-890°C [32]	prograde-peak	UH*P* Grt, Qtz and Ap in UH*P* Grt	high-salinity brine inclusions		unidentified						halite			yes			high-salinity brines
	UH*P* eclogite [32]	3.0 - 4.5 GPa 700-850°C [33]	prograde-peak	Qtz in UH*P* Grt	CH_4-rich inclusions												$CH_4 \pm N_2$		CH_4-rich fluids
	eclogite [34]	3.0 - 4.5 GPa 700-850°C [33]	retrograde	UH*P* Grt and Omp	polyphase inclusions		k-feldspar quartz albite												hydrous Na-K-Al-Si melt produced during dehydration melting of mica
	OH-rich Toz - Ky quartzite [35, 36]	3.0 - 4.5 GPa 700-850°C [33]	peak	UH*P* Ky	multiphase-solid inclusions	paragonite muscovite chlorite	SiO_2 zircon	calcite	anhydrite alunite-type sulphate barite	pyrite		corundum						yes	supercritical silicate-rich aqueous fluid / intermediate alkali-alumino-silicate aqueous solutions
	OH-rich Toz - Ky quartzite [35, 36]	3.0 - 4.5 GPa 700-850°C [33]	retrograde	H*P* Toz	aqueo-carbonic fluid inclusions				gypsum anhydrite				halite			yes	CO_2		$CaCl_2$-rich brines
	Ky-Phe-Ep eclogite [35, 37]	3.0 - 4.5 GPa 700-850°C [33]	peak	UH*P* Grt and Ky	multiphase-solid inclusions	paragonite amphibole Zn-staurolite	plagioclase		alunite-type sulphate	pyrite	apatite	rutile magnetite Zn-Mg-Al-Fe-Ti spinel						yes	supercritical silicate-rich fluid aqueous
	Ky-Phe-Ep eclogite [35, 37]	3.0 - 4.5 GPa 700-850°C [33]	retrograde	UH*P* Ep and Ky	bi-phase aqueous inclusions			Mg-calcite								yes			Na-Ca brine
	Ky-Phe-Ep eclogite [35, 37]	3.0 - 4.5 GPa 700-850°C [33]	retrograde	H*P* Ep, Qtz	three-phase aqueous inclusions								salts			yes			Na-brine

[a] all the inclusions considered in this work were trapped at UHP conditions or at the HP-UHP or UHP-HP transition
[b] mineral abbreviations after Kkretx (1983) and Whitney & Evans (2010)
[27] Gao et al. (2012), [28] Liu et al. (2013), [29] Xiao et al. (2000), [30] Fu et al. (2001), [31] Xiao et al. (2002), [32] Fu et al. (2003a), [33] Zhang et al. (2008), [34] Zeng et al. (2009), [35] Ferrando et al. (2005b), [36] Frezzotti et al. (2007), [37] Ferrando et al. (2005a)

Table 1. continue

Metamorphic Belt	Lithology	Peak *P-T* conditions	Trapping conditions [a]	Host mineral [b]	Name of the inclusions	silicates (hydrous)	silicates	carbonates	sulphates	sulphides	phosphates	oxides	chlorides	C phases	glass	water	gas	empty cavities	
Continental crust																			
Dabie-Sulu	Qtz vein in eclogite [38]	3.0 - 4.5 GPa 700-850°C [33]	retrograde	Qtz	gas-rich inclusions												N_2 CH_4		H_2-CH_4 fluids
	eclogite and Ky-quartzite [39, 40]	3.0 - 4.5 GPa 700-850°C [33]	peak	UH*P* Grt, Omp and Ky	high-salinity H_2O inclusions	amphibole mica	zircon	carbonate		pyrite		opaque minerals	halite			brine			multicomponent brine
	eclogite and veins [33]	3.0 - 4.5 GPa 700-850°C [33]	peak	UH*P* Zo and Ky	multiphase solid inclusions	paragonite		carbonate	anhydrite	pyrite		corundum magnetite				yes		yes	silicate-rich supercritical fluid
	eclogite and veins [33]	3.0 - 4.5 GPa 700-850°C [33]	peak	UH*P* Aln and Zo	multi-solid fluid inclusions	paragonite muscovite	quartz	calcite	anhydrite celestite		apatite					yes			silicate-rich supercritical fluid
	eclogite [41]	3.0 - 4.5 GPa 700-850°C [33]	peak	UH*P* Omp and Grt	multi-phase aqueous inclusions	amphibole mica		calcite				oxides	halite			yes			high-density brine
	granulitized UH*P* eclogite [42]	3.0 - 4.5 GPa 700-850°C [33]	prograde-peak	UH*P* Grt	N_2±H_2O inclusions								halite			brine	N_2		H_2-fluids coeval with high-salinity brines
Greenland Caledonides	metapelites [43]	3.6 GPa 970°C [43]	retrograde	UH*P* Grt	polyphase inclusions	phengite biotite	quartz kyanite K-feldspar plagioclase					rutile							melt from dehydration melting of phengite
Mantle																			
Betic Cordillera	Ol-Opx rocks [44]	1.5 - 2.2 GPa 640 - 750°C [44]	peak	H*P* Ol	fluid + mineral inclusions	chlorite	olivine				Cl-apatite	magnetite				yes			homogeneous (supercritical?) fluid loaded of dissoved components
Western Gneiss Region	Grt websterite [45, 46, 47]	3.9 - 4.3 GPa 850-900°C [45]	peak	UH*P* Spl, Opx, Cpx and Grt	multiphase solid inclusions	phlogopite	zircon kalisilite orthopyroxene	magnesite $(BaCa)CO_3$ dolomite		Fe-Ni-sulphide Ba-sulphide	Cl-apatite monazite	Cr-spinel rutile periclase		diamond C-phase					COH- and silicate-rich supercritical fluid
	Grt websterite [48]	5.5 GPa 800°C [48]	peak	UH*P* Grt	polyphase solid inclusions	amphibole chlorite	Al-silicate			Fe-Pb-sulphides	Y-phosphate	Al-Fe-Mg oxides Al-spinel		diamond C-phase					supercritical, dense, H-C-N-O-F-P-S-Cl metal-bearing supercritical fluids
Moldanubian Zone	Phl-Ap-bearing Spl-Grt peridotite [49]	2.3 - 3.5 GPa 850 - 1030°C [49]	peak	UH*P* Cr-Spl	multiphase solid inclusions	phlogopite chlorite Mg-hornblende talc		dolomite calcite		Fe-Ni sulphide galena	apatite monazite	U-Th oxide		graphite					carbonatite melt or supercritical fluid
	Grt pyroxenite [29, 50]	ca 2.0 GPa 680-860°C [50]	prograde-peak	UH*P* Grt	high-salinity aqueous inclusions ± N_2								halite			yes	H_2 ± CO_2		N_2-bearing NaCl-rich solutions
Dabie-Sulu	Grt orthopyroxenite and Grt-websterite [51, 52]	3.9 - 4.1 GPa 700 - 800°C [51]	peak	UH*P* Grt	polyphase inclusions	amphibole chlorite talc mica	albite sphene			sulfide	apatite	spinel							solute-rich aqueous fluids
	Grt-peridotite [52]	ca 4.2 GPa ca 760°C [52]	peak	UH*P* Grt	polyphase inclusions	amphibole chlorite talc mica				pyrite		spinel							solute-rich aqueous fluids

[a] all the inclusions considered in this work were trapped at UHP conditions or at the HP-UHP or UHP-HP transition
[b] mineral abbreviations after Kkretx (1983) and Whitney & Evans (2010)
[38] Xu et al. (2006), [39] Zhang et al. (2005), [40] Xiao et al. (2006), [41] Shen et al. (2003), [42] Fu et al. (2003b),
[43] Lang & Gilotti (2007), [44] Scambelluri et al. (2001), [45] Carswell and van Roermund (2005),
[46] van Roermund et al. (2002), [47] Malaspina et al. (2010), [48] Vrijmoed et al. (2008), [49] Naemura et al. (2009),
[50] Xiao et al. (2001), [51] Malaspina et al. (2006), [52] Malaspina et al. (2009)

Table 1

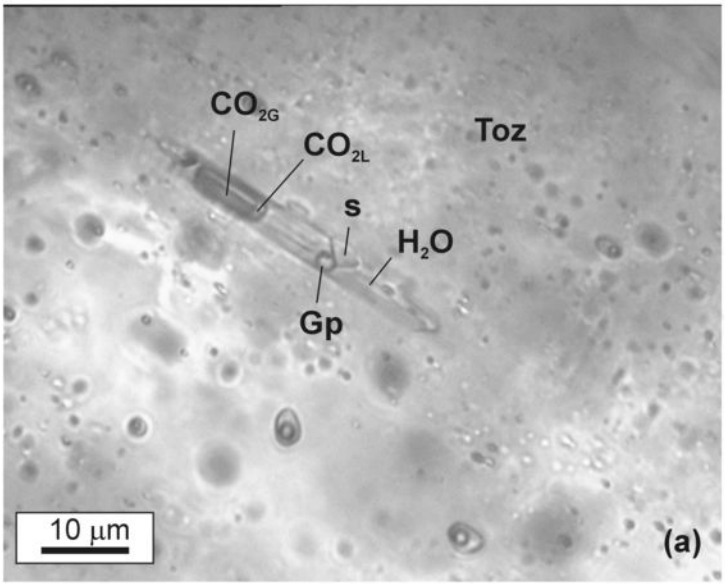
CO_{2G}
CO_{2L}
Toz
s
H_2O
Gp
10 μm
(a)

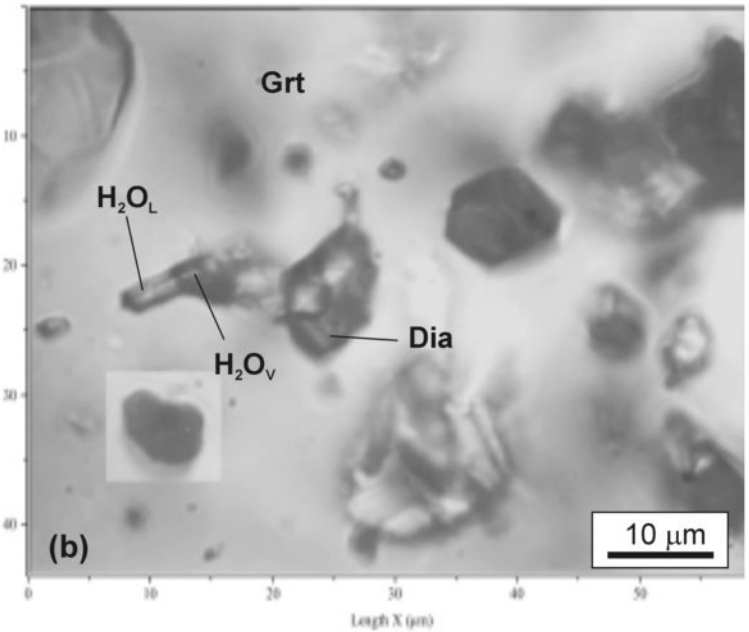
Grt
H_2O_L
Dia
H_2O_V
10 μm
(b)
Length X (μm)

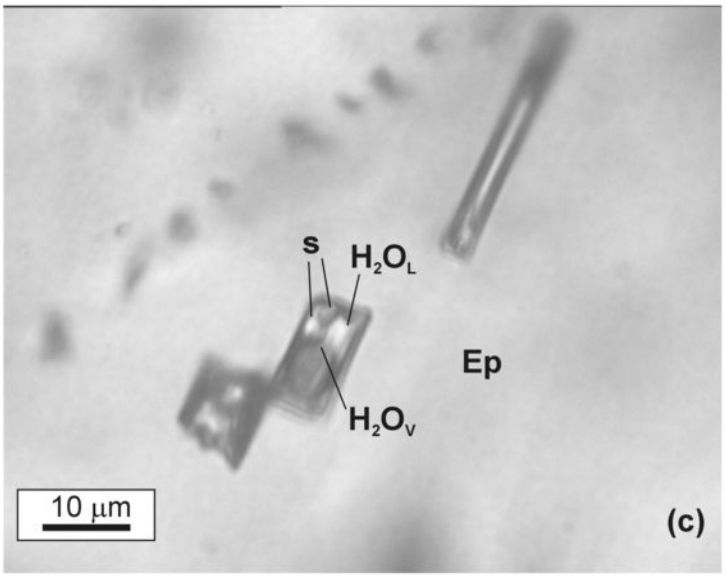
s
H_2O_L
Ep
H_2O_V
10 μm
(c)

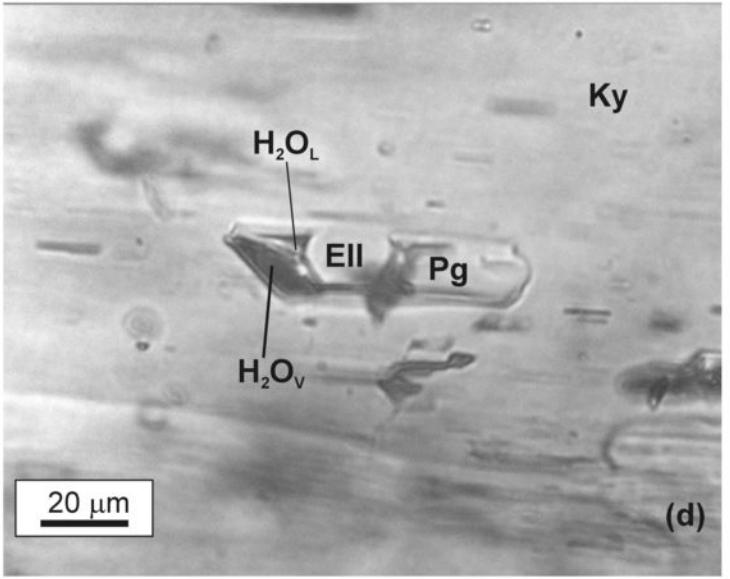
Ky
H_2O_L
Ell
Pg
H_2O_V
20 μm
(d)

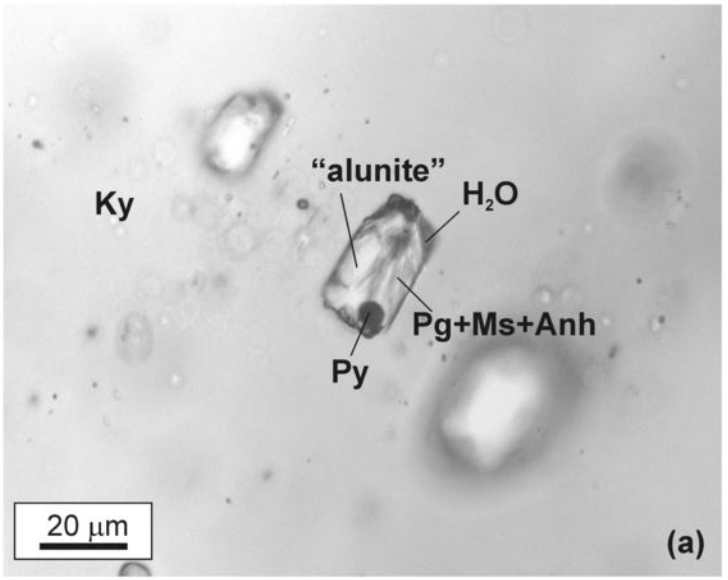
Ky
"alunite"
H_2O
Pg+Ms+Anh
Py
20 μm
(a)

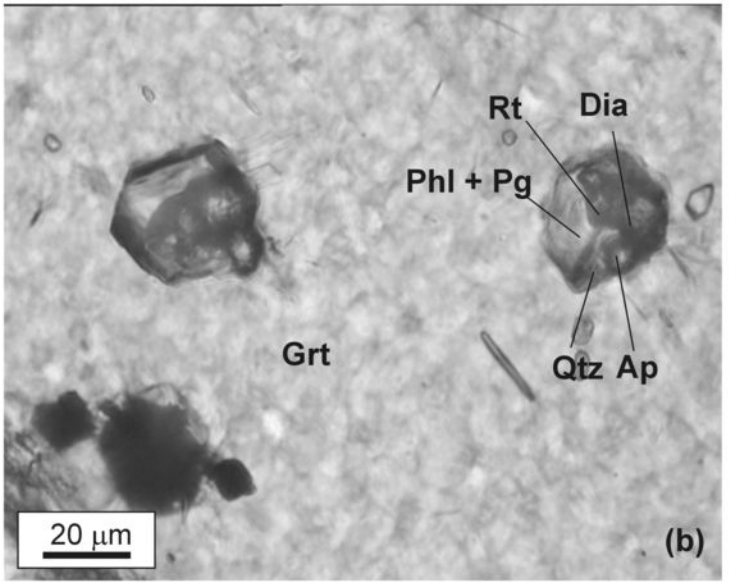
Rt
Dia
Phl + Pg
Grt
Qtz
Ap
20 μm
(b)

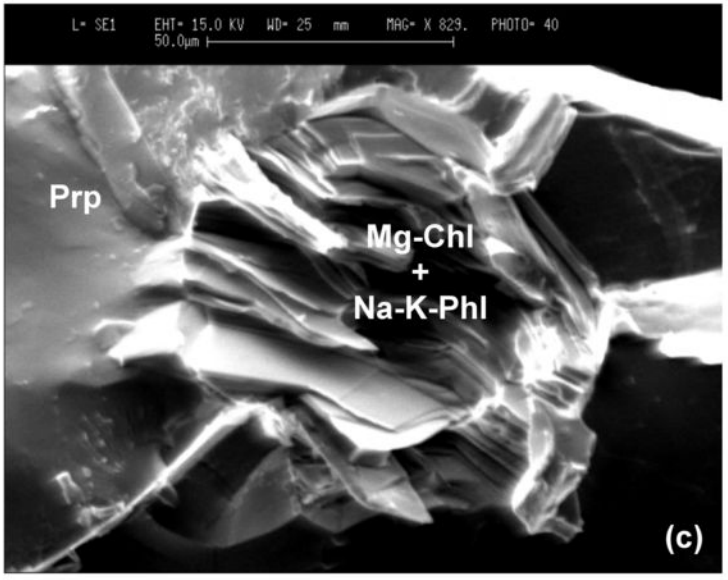
L= SE1 EHT= 15.0 KV WD= 25 mm MAG= X 829. PHOTO= 40
50.0μm
Prp
Mg-Chl
+
Na-K-Phl
(c)

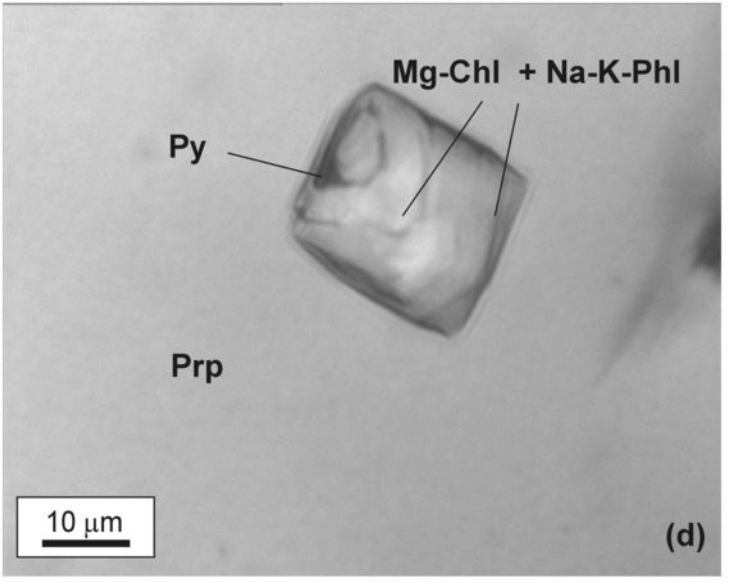
Mg-Chl + Na-K-Phl
Py
Prp
10 μm
(d)

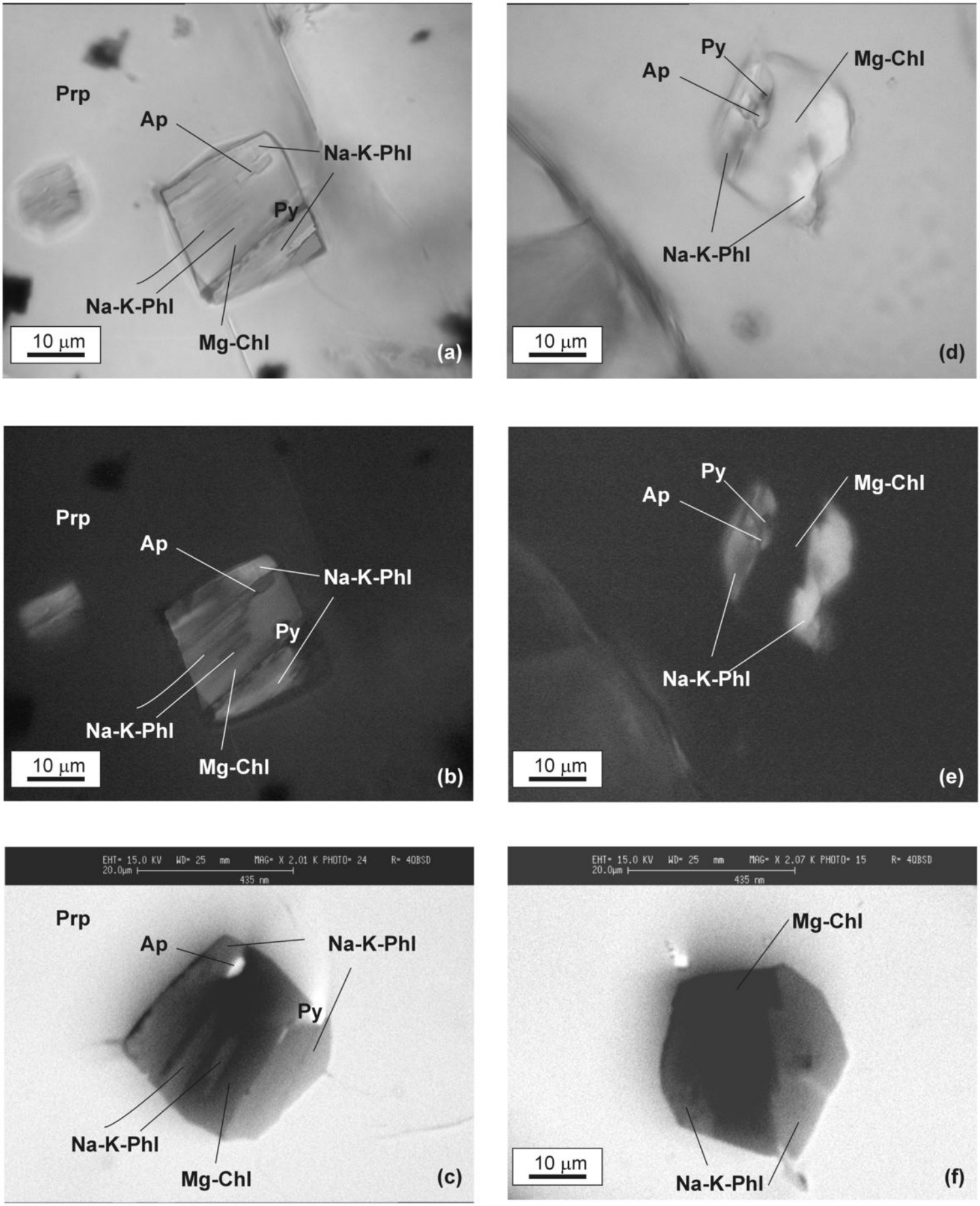
Prp
Ap
Na-K-Phl
Py
Na-K-Phl
Mg-Chl
10 μm
(a)
Py
Ap
Mg-Chl
Na-K-Phl
10 μm
(d)
Prp
Ap
Na-K-Phl
Py
Na-K-Phl
Mg-Chl
10 μm
(b)
Py
Ap
Mg-Chl
Na-K-Phl
10 μm
(e)
EHT= 15.0 KV WD= 25 mm MAG= X 2.01 K PHOTO= 24 R= 40BSD
20.0μm
435 nm
Prp
Ap
Na-K-Phl
Py
Na-K-Phl
Mg-Chl
(c)
EHT= 15.0 KV WD= 25 mm MAG= X 2.07 K PHOTO= 15 R= 40BSD
20.0μm
435 nm
Mg-Chl
10 μm
Na-K-Phl
(f)

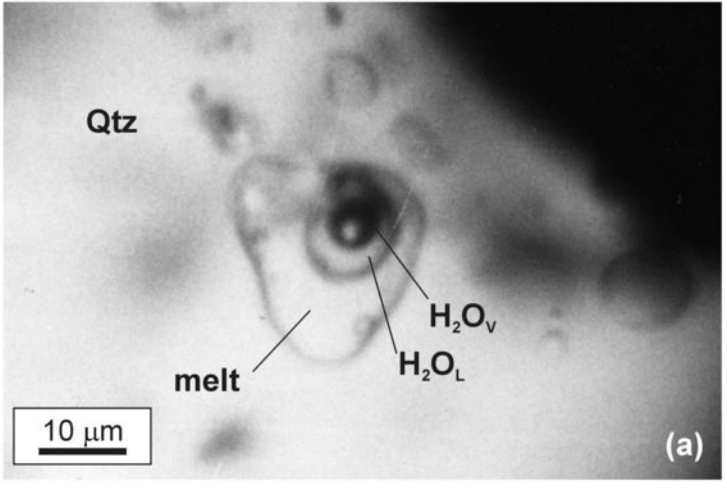
Qtz
H_2O_V
H_2O_L
melt
10 μm
(a)

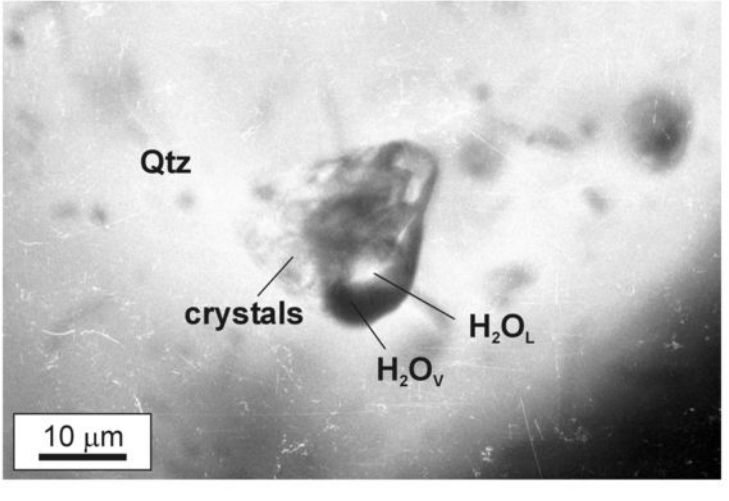
Qtz
crystals
H_2O_L
H_2O_V
10 μm

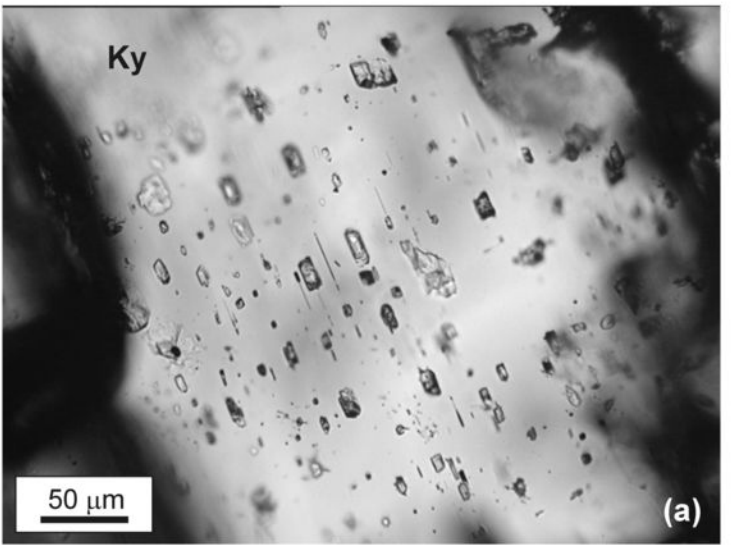
Ky
50 μm
(a)

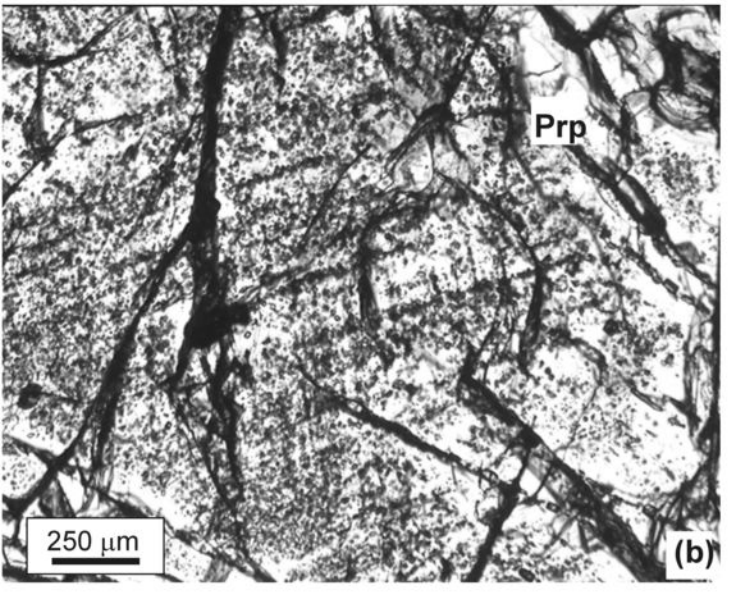
Prp
250 μm
(b)

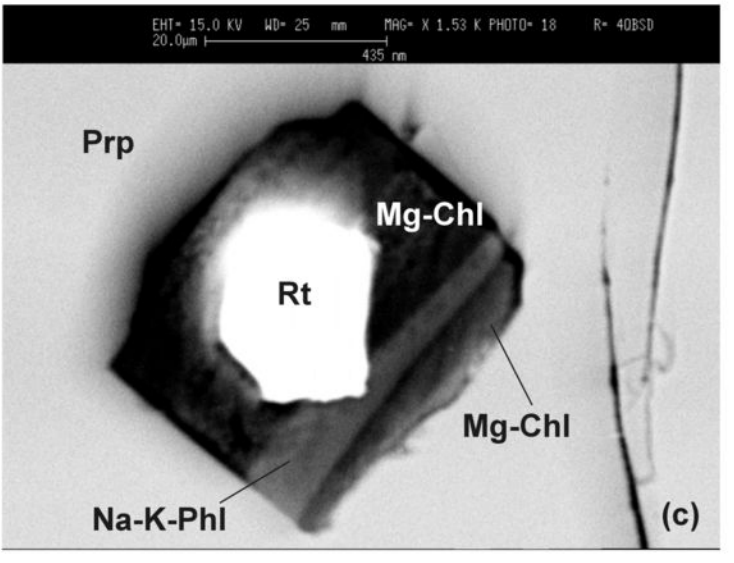
EHT= 15.0 KV WD= 25 mm MAG= X 1.53 K PHOTO= 18 R= 40BSD
20.0μm
435 nm
Prp
Mg-Chl
Rt
Mg-Chl
Na-K-Phl
(c)

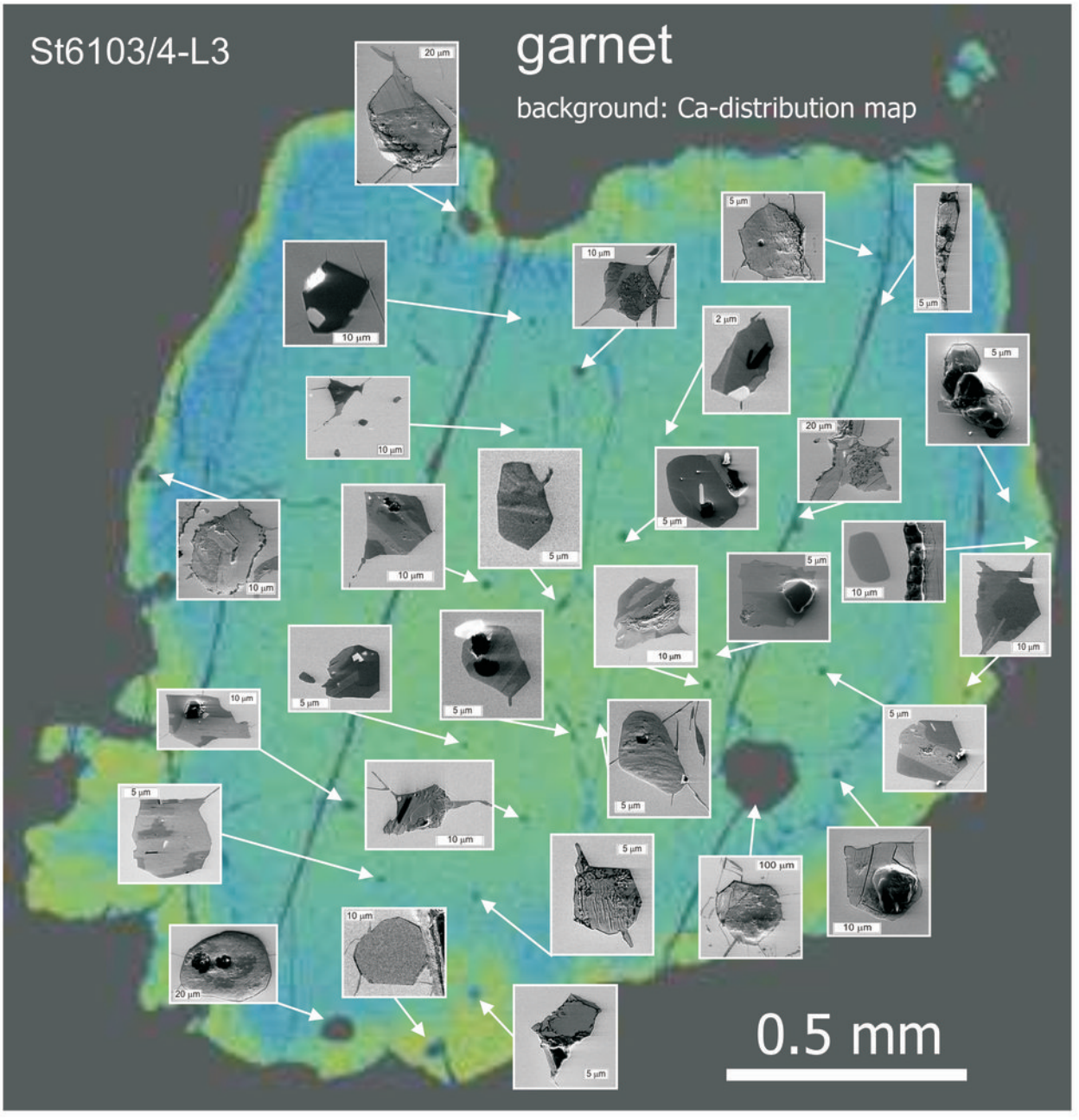
St6103/4-L3
garnet
background: Ca-distribution map
20 µm
10 µm
5 µm
10 µm
10 µm
2 µm
5 µm
10 µm
20 µm
5 µm
10 µm
5 µm
10 µm
5 µm
10 µm
10 µm
5 µm
5 µm
10 µm
5 µm
5 µm
10 µm
5 µm
5 µm
100 µm
10 µm
10 µm
20 µm
5 µm
0.5 mm

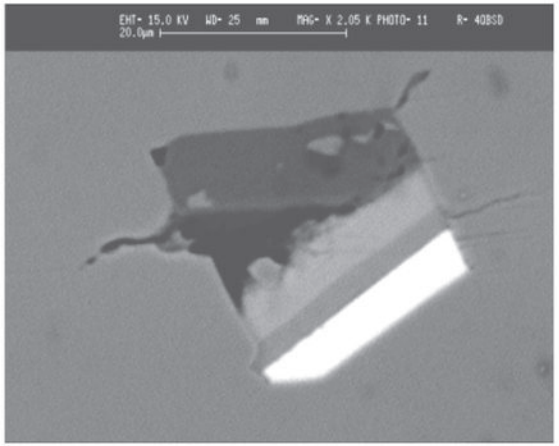

1

2

$\Delta P > 0$

3

offshoots

water diffusion in the host mineral

4

$\Delta P > 0$

5

microfractures with trails and clusters of fluid inclusions

HP ⟶ UHP

Temperature

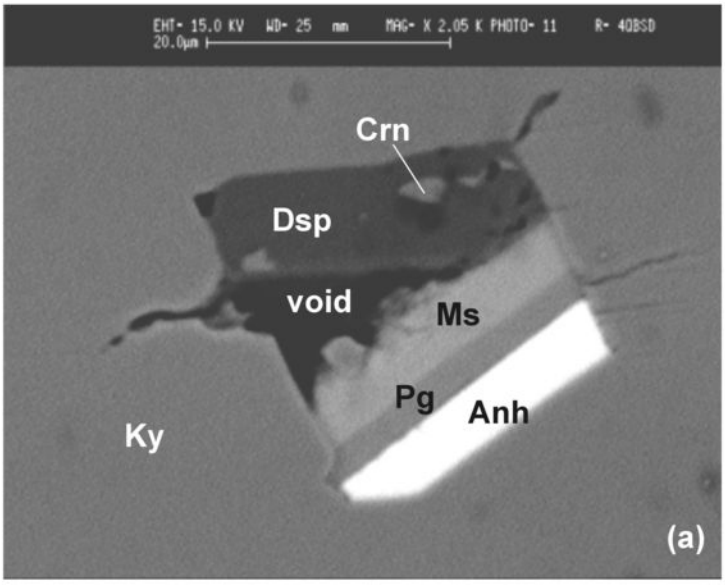
EHT- 15.0 KV WD- 25 mm MAG- X 2.05 K PHOTO- 11 R- 4QBSD
20.0µm
Crn
Dsp
void
Ms
Pg
Anh
Ky
(a)

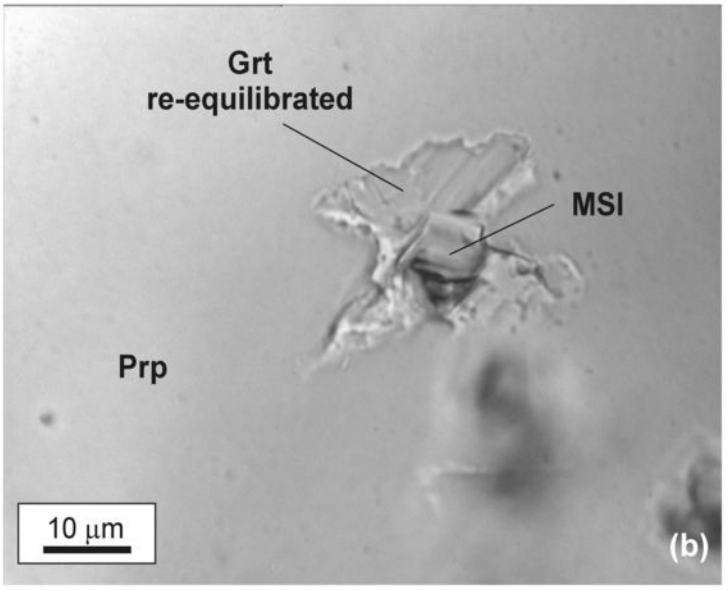
Grt
re-equilibrated
MSl
Prp
10 µm
(b)

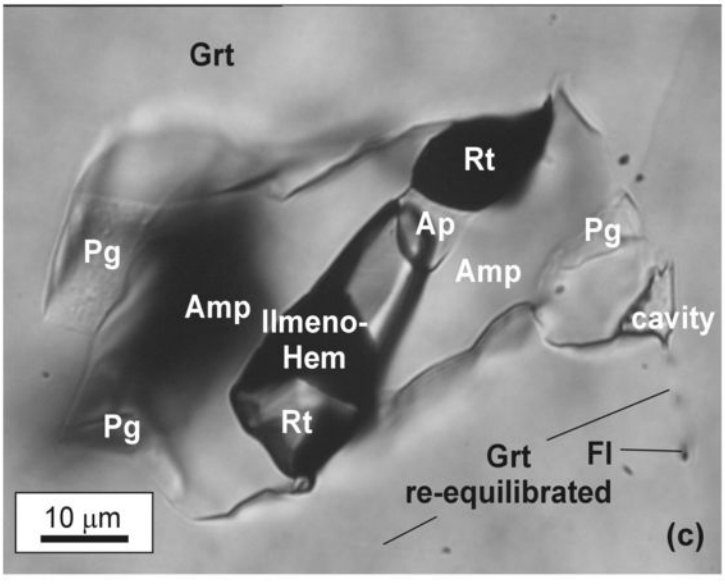
Grt
Rt
Ap
Pg
Pg
Amp
Amp
Ilmeno-
Hem
cavity
Pg
Rt
Grt
re-equilibrated
Fl
10 µm
(c)

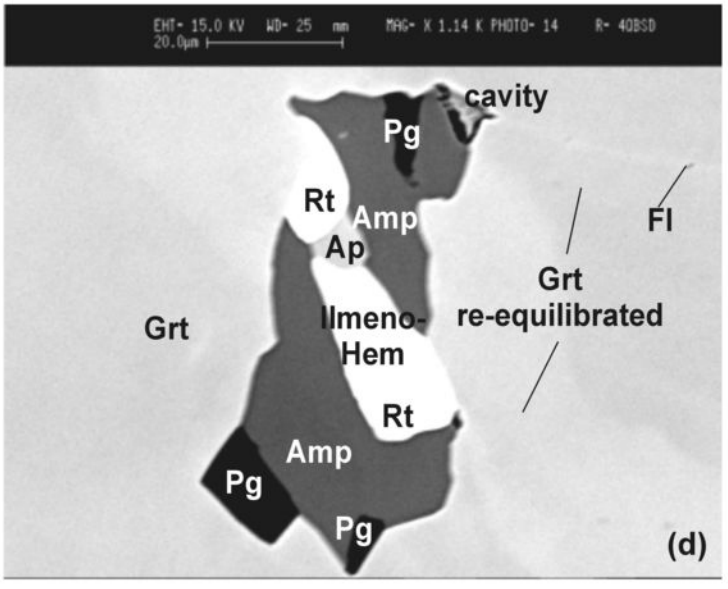
EHT- 15.0 KV WD- 25 mm MAG- X 1.14 K PHOTO- 14 R- 4QBSD
20.0µm
cavity
Pg
Rt
Amp
Ap
Fl
Grt
re-equilibrated
Grt
Ilmeno-
Hem
Rt
Amp
Pg
Pg
(d)

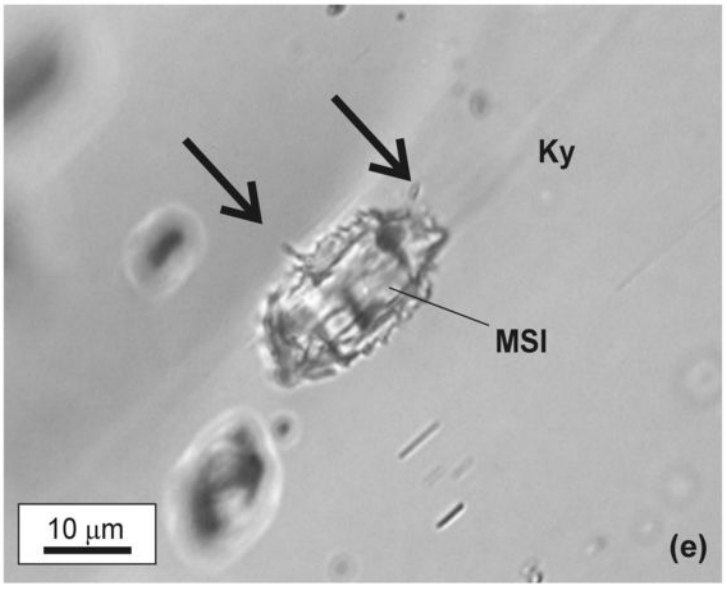
Ky
MSl
10 µm
(e)

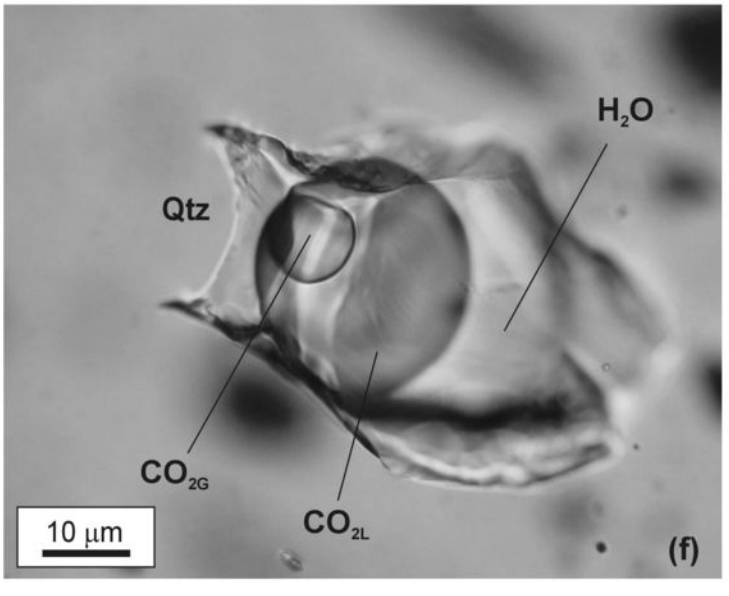
H2O
Qtz
CO2G
CO2L
10 µm
(f)

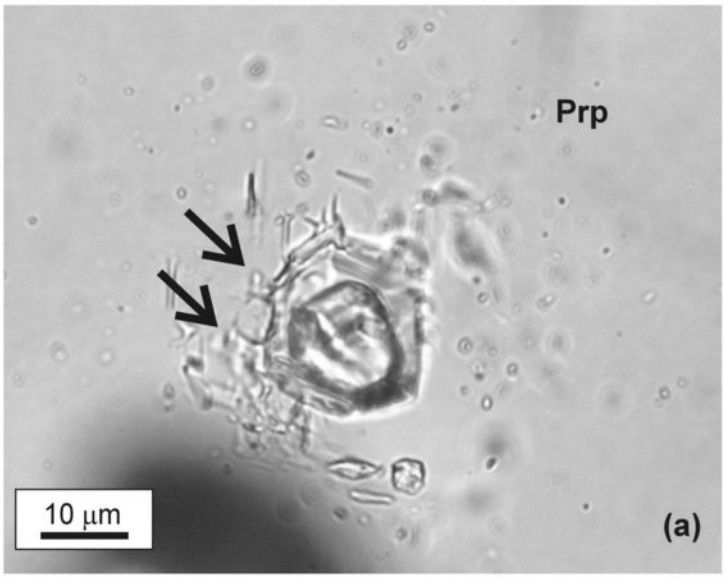
Prp
10 μm
(a)

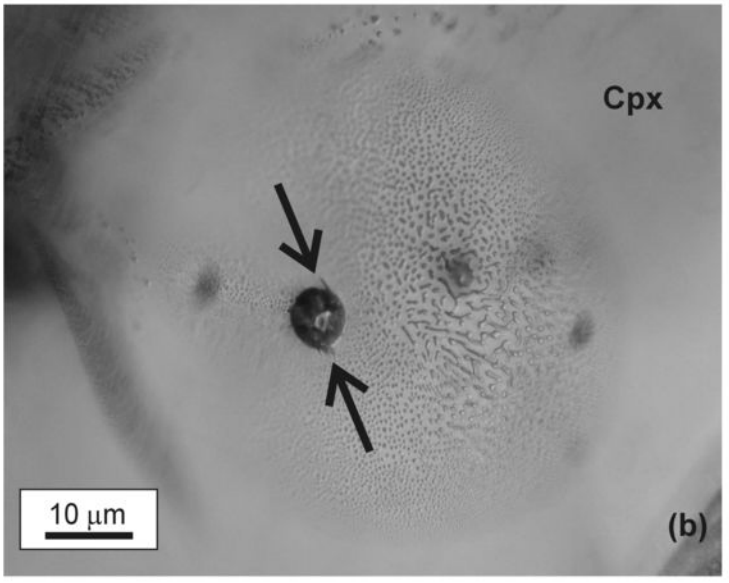
Cpx
10 μm
(b)

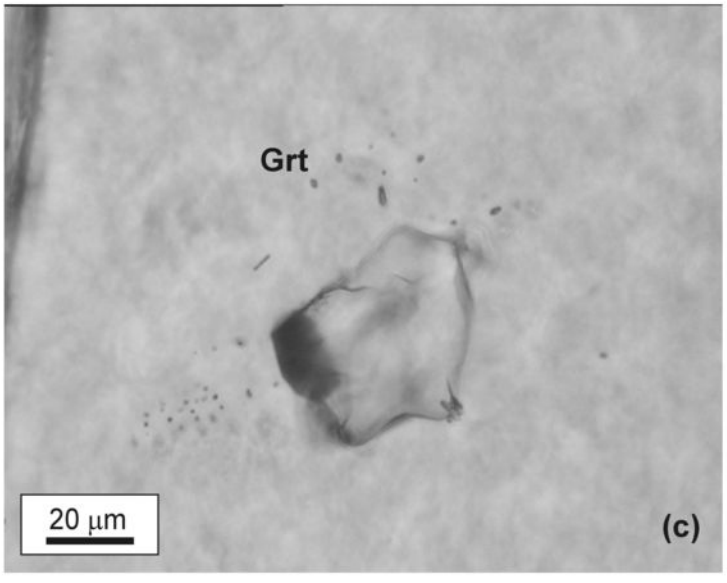
Grt
20 μm
(c)

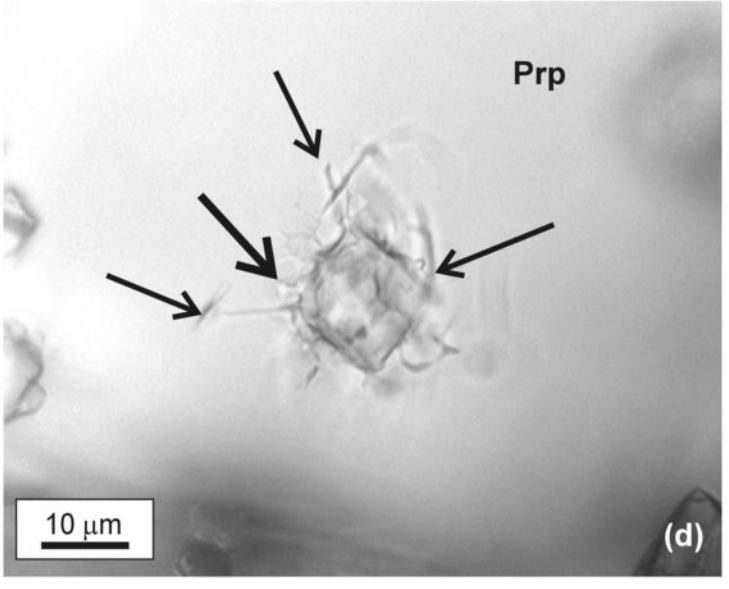
Prp
10 μm
(d)

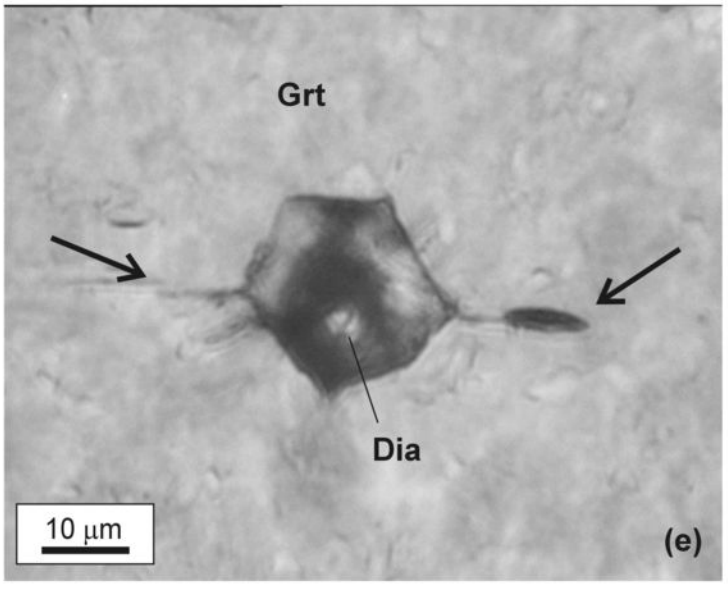
Grt
Dia
10 μm
(e)

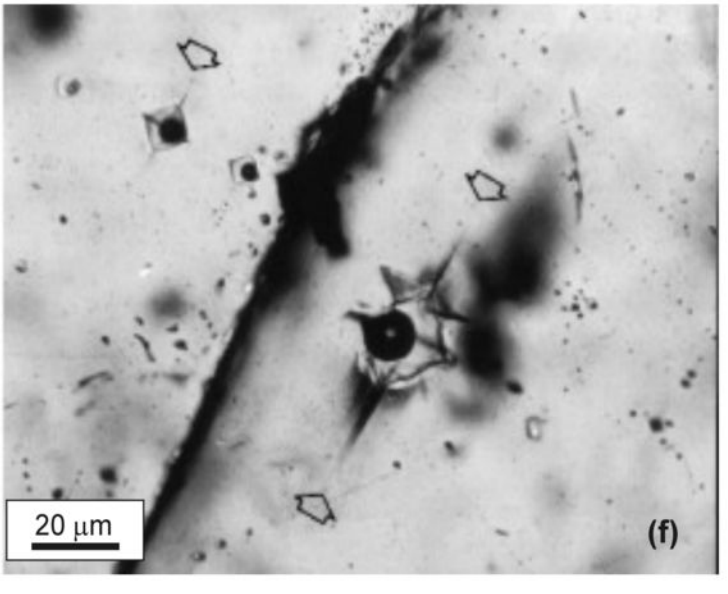
20 μm
(f)

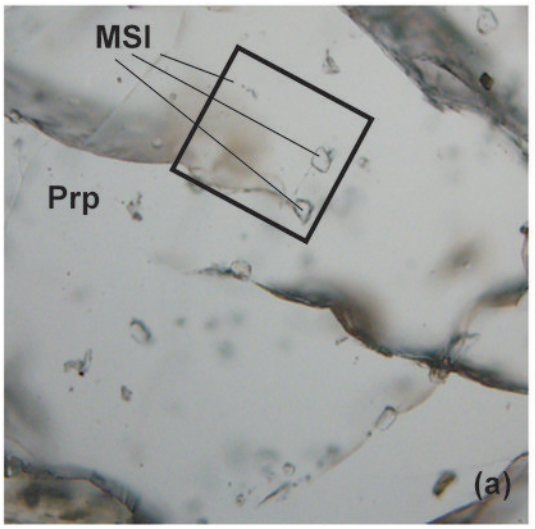
MSI
Prp
(a)

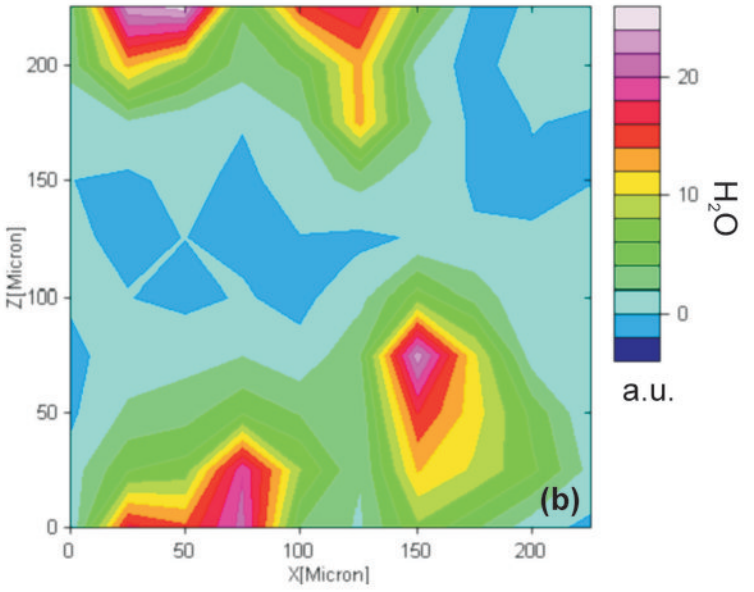
Z[Micron]
X[Micron]
(b)
H2O
a.u.

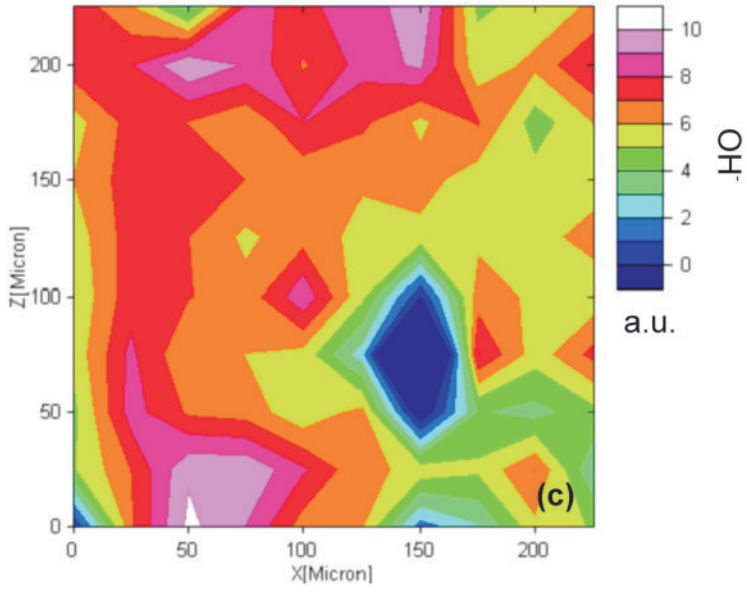
Z[Micron]
X[Micron]
(c)
OH-
a.u.

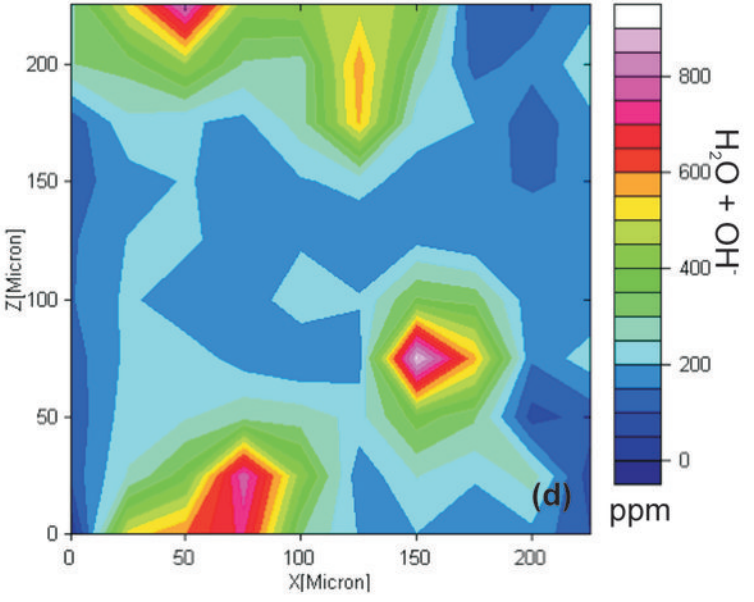
Z[Micron]
X[Micron]
(d)
H2O + OH-
ppm

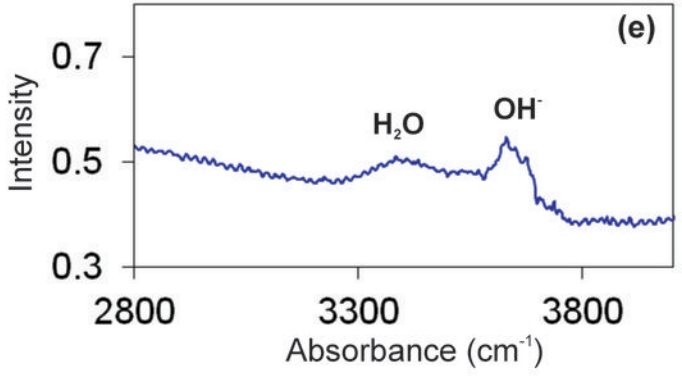
(e)
Intensity
H2O
OH-
Absorbance (cm-1)

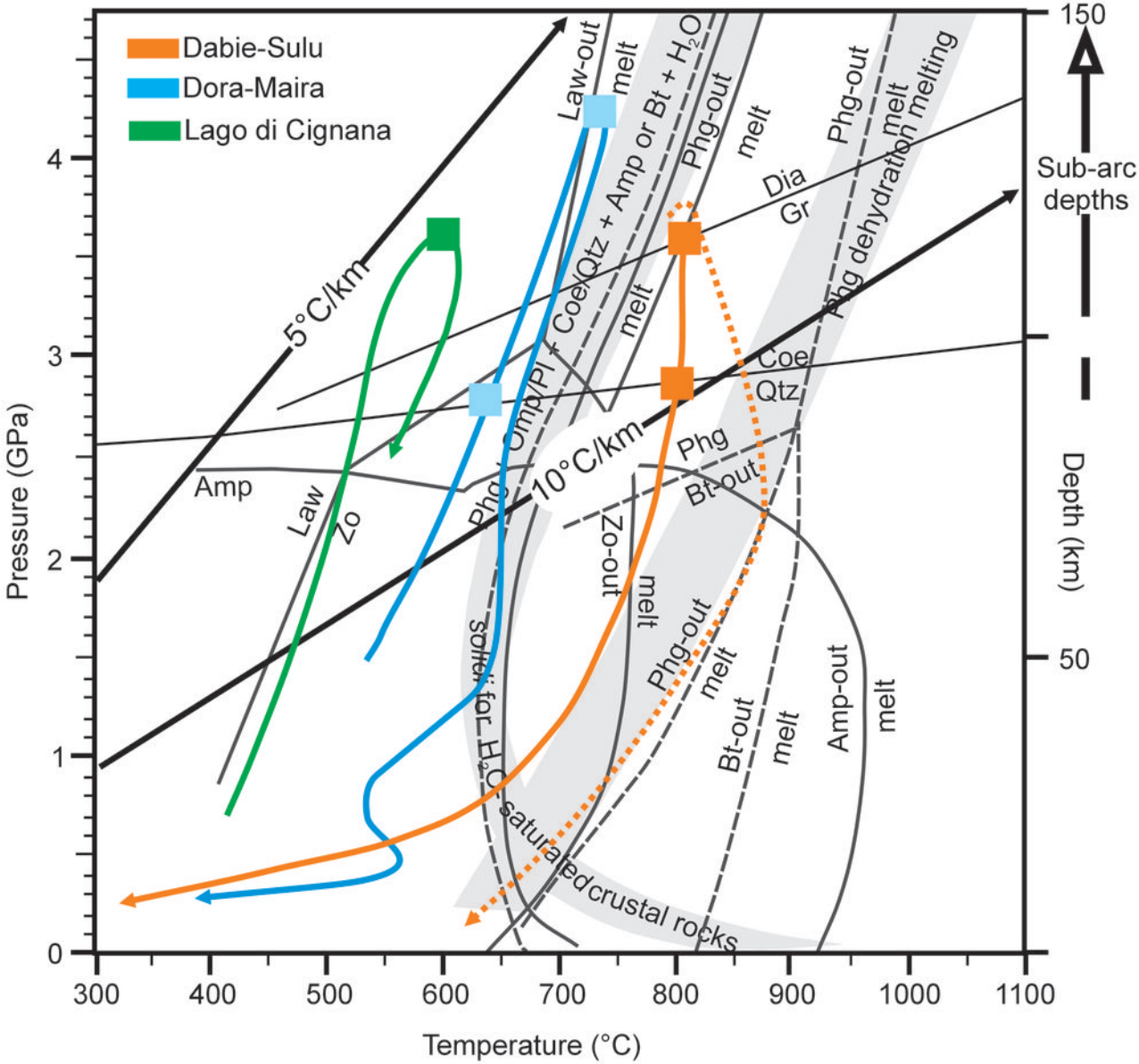
Dabie-Sulu
Dora-Maira
Lago di Cignana
5°C/km
10°C/km
Law-out
melt
Phg-out
melt
Phg-out
melt
Phg dehydration melting
Dia
Gr
Coe
Qtz
Coe/Qtz + Amp or Bt + H2O
melt
Omp/Pl + Coe/Qtz
Amp
Law
Zo
Phg
Bt-out
Zo-out
melt
Phg-out
melt
Bt-out
melt
Amp-out
melt
solidus for H2O saturated crustal rocks
Sub-arc depths
Depth (km)
150
50
Pressure (GPa)
Temperature (°C)
0
1
2
3
4
300
400
500
600
700
800
900
1000
1100

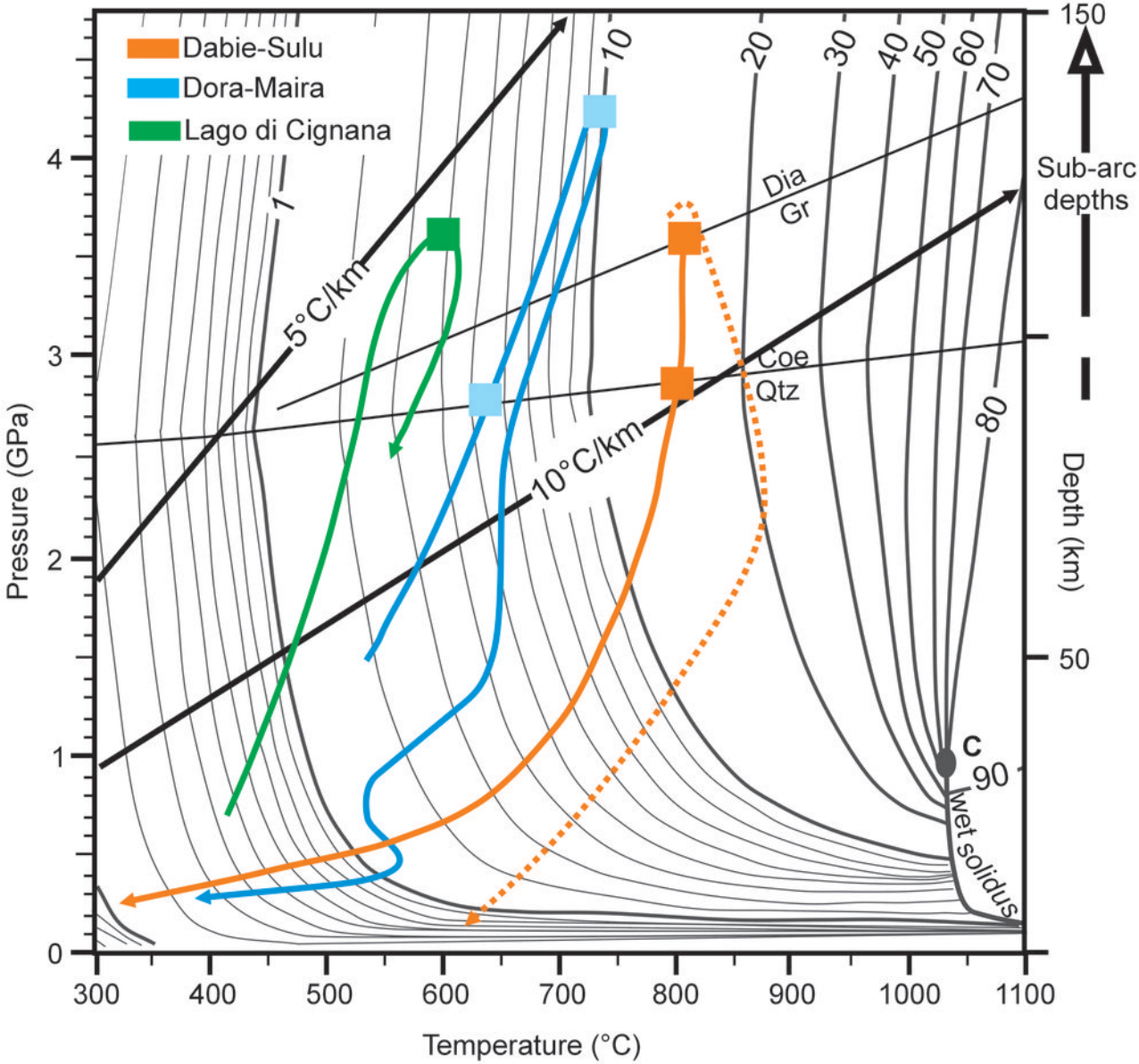
Dabie-Sulu
Dora-Maira
Lago di Cignana
1
10
20
30
40
50
60
70
80
90
Dia
Gr
Coe
Qtz
5°C/km
10°C/km
wet solidus
Sub-arc depths
150
50
Depth (km)
Pressure (GPa)
Temperature (°C)
0
1
2
3
4
300
400
500
600
700
800
900
1000
1100

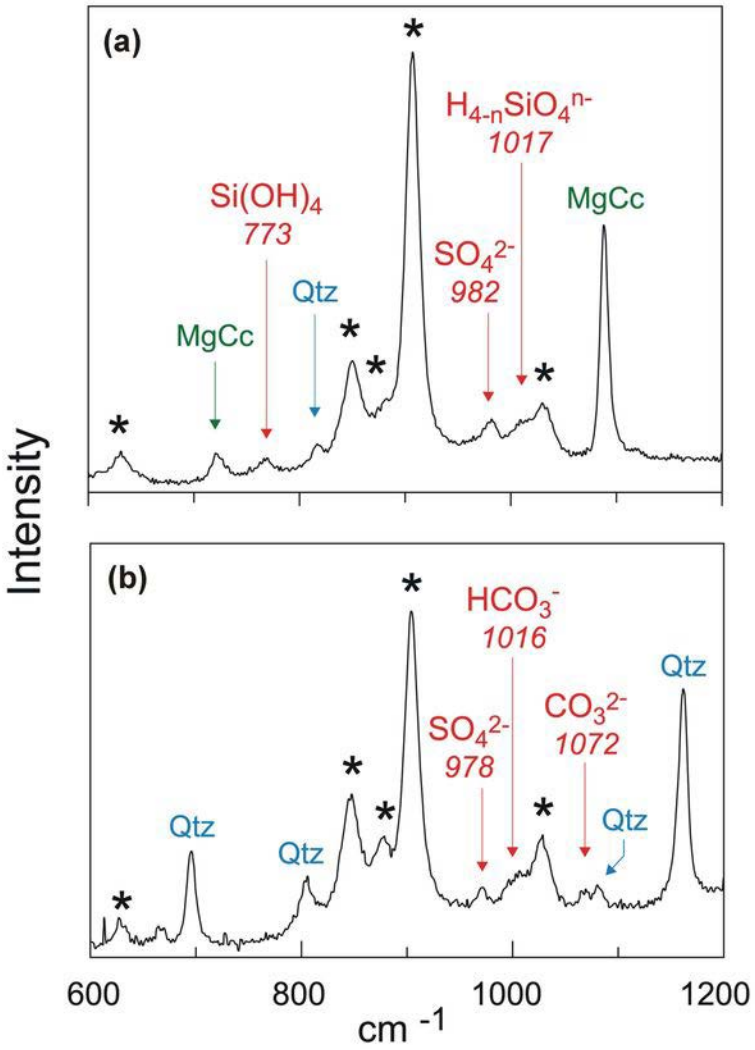
(a)
$H_{4-n}SiO_4^{n-}$
1017
$Si(OH)_4$
773
MgCc
SO_4^{2-}
982
Qtz
MgCc
(b)
HCO_3^-
1016
Qtz
SO_4^{2-}
978
CO_3^{2-}
1072
Qtz
Qtz
Qtz
Intensity
600
800
1000
1200
cm -1

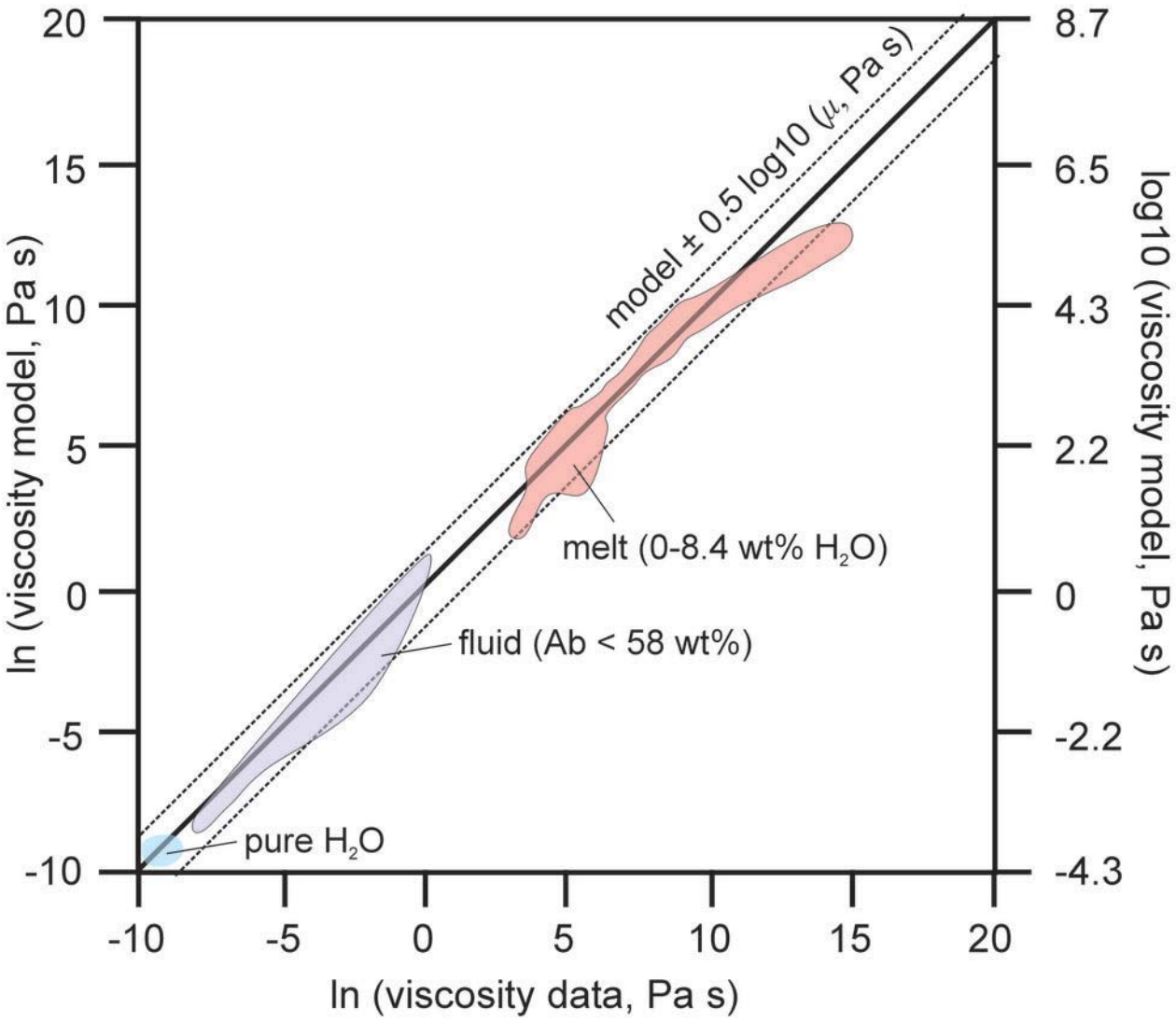
20
15
10
5
0
-5
-10
8.7
6.5
4.3
2.2
0
-2.2
-4.3
-10
-5
0
5
10
15
20
ln (viscosity model, Pa s)
log10 (viscosity model, Pa s)
ln (viscosity data, Pa s)
model ± 0.5 log10 (μ, Pa s)
melt (0-8.4 wt% H2O)
fluid (Ab < 58 wt%)
pure H2O

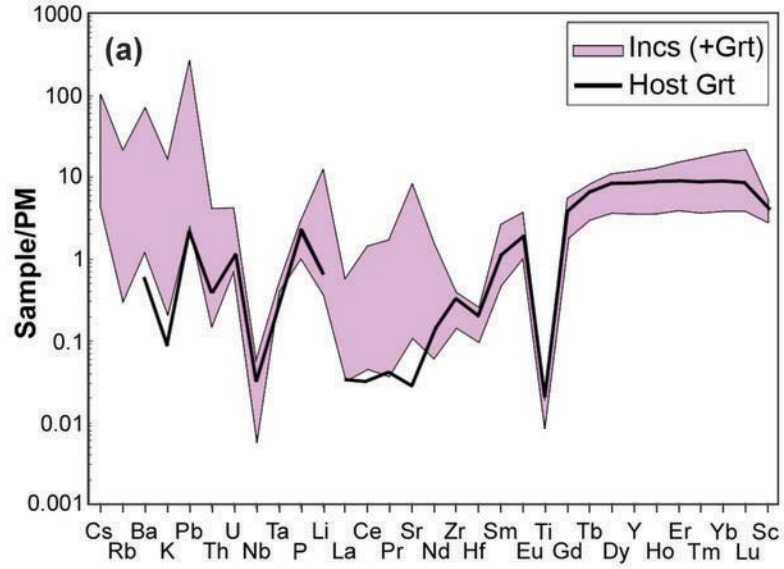
(a)
Incs (+Grt)
Host Grt
Sample/PM
1000
100
10
1
0.1
0.01
0.001
Cs Ba Pb U Ta Li Ce Sr Zr Sm Ti Tb Y Er Yb Sc
Rb K Th Nb P La Pr Nd Hf Eu Gd Dy Ho Tm Lu

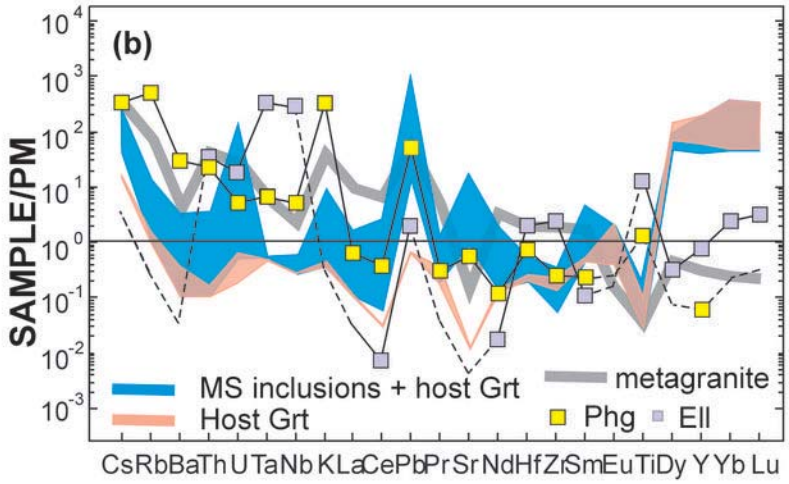
(b)
SAMPLE/PM
MS inclusions + host Grt
Host Grt
metagranite
Phg
Ell
CsRbBaTh U TaNb K LaCePbPr Sr NdHfZrSmEuTiDy Y Yb Lu